Understanding which parameters control shallow ascent of silicic effusive magma

Mark E. Thomas[1] and Jurgen W. Neuberg[1]

[1]Institute of Geophysics and Tectonics, School of Earth and Environment, University of Leeds, Leeds, UK

Abstract The estimation of the magma ascent rate is key to predicting volcanic activity and relies on the understanding of how strongly the ascent rate is controlled by different magmatic parameters. Linking potential changes of such parameters to monitoring data is an essential step to be able to use these data as a predictive tool. We present the results of a suite of conduit flow models Soufrière that assess the influence of individual model parameters such as the magmatic water content, temperature or bulk magma composition on the magma flow in the conduit during an extrusive dome eruption. By systematically varying these parameters we assess their relative importance to changes in ascent rate. We show that variability in the rate of low frequency seismicity, assumed to correlate directly with the rate of magma movement, can be used as an indicator for changes in ascent rate and, therefore, eruptive activity. The results indicate that conduit diameter and excess pressure in the magma chamber are amongst the dominant controlling variables, but the single most important parameter is the volatile content (assumed as only water). Modeling this parameter in the range of reported values causes changes in the calculated ascent velocities of up to 800%.

1. Introduction

A volcanic conduit provides the pathway for transport of magma and magmatic fluids within a volcano and it is possible to detect this movement through geophysical monitoring such as seismicity and ground deformation [e.g., *Neuberg et al.*, 2006; *Zobin et al.*, 2011; *Lopez et al.*, 2013]. However, the extent to which changes in magma flow properties affect the data recorded on volcanoes is not well defined. Is it possible that a small change in magma temperature or water content could alter the flow within the conduit enough to be recorded by geophysical monitoring instruments or simple visual observation? What effect does the size of gas bubbles within the magma have on the overall flow dynamics and how big do these changes need to be to alter the eruption style? These types of question are addressed within this study in an attempt to identify the crucial parameters that cause changes in observed volcanic behavior.

Here we use conduit flow models to analyze the key input parameters that control magma flow properties, such as the magma water content, crystal content and conduit geometry, and use the numerical simulations to assess their relative importance to the overall magma flow dynamics. A list of all input parameters is presented in Table 1 along with the range of values studied. We focus on evolved silicic magmatic systems because of the wealth of relevant information and previous numerical modeling attempts relating to Soufrière Hills Volcano, Montserrat, a long lived andesitic dome forming eruption [*Sparks et al.*, 2000] and excellent natural laboratory. While the initial models are based on extrusive eruptions the results of changing the model parameters have the potential to alter the eruption style and it is noted that the underlying principles discussed here are applicable to other volcanic systems.
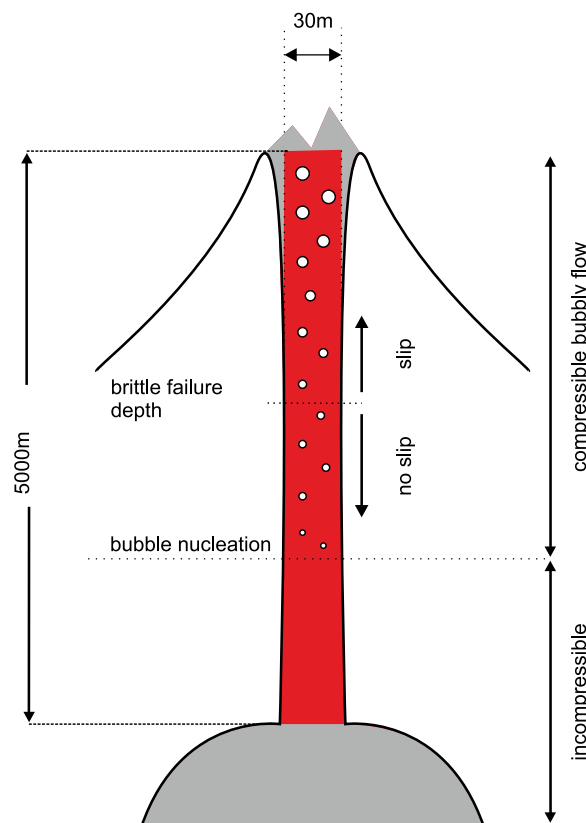
2. The Model

The conduit flow models are based on an updated approach of *Collier and Neuberg* [2006] outlined in *Thomas and Neuberg* [2012]. Conduit flow is computed through the use of the finite element modeling package COMSOL Multiphisics®. The models are built as cylindrical conduits within an axial symmetric domain space to minimize computing requirements. The mesh consists of approx. 60 000 elements with a maximum node spacing of 2.75 m and a layer of four boundary elements of 0.2 m thickness near the conduit wall.

Table 1. Parameters Used in the Reference Model and Range of Parameter Variations Which are Discussed in Section 3.4

Symbol/ Abbreviation	Variable	"Reference" Model Value	Range of Modeled Values
	The melt composition	Rhyolitic ($>71\%$ SiO$_2$) [*Barclay et al.*, 1998]	See Table 2
b_{ni}	Bubble number density	10^{10} m^{-3} [*Cluzel et al.*, 2008]	10^7-10^{11} m^{-3}
D_{TBL}	Thickness of thermal boundary layer over which T_{diff} is lost	0.3 m [*Collier and Neuberg*, 2006]	0.3–0.5 m
Γ	Bubble surface tension	0.06 Nm^{-1} [*Lyakhovsky et al.*, 1996]	0.05–0.25 Nm^{-1}
χ_c	Magma chamber crystal volume fraction	40% [*Barclay et al.*, 1998]	40–50%
Ls	Slip length of brittle failure of melt	0.01	0.01–1.0 m
P_e	Excess chamber pressure above lithostatic	0 MPa	0–20 MPa
P_{top}	Pressure at conduit exit	0.09 MPa	0.09–4.5 MPa
ρ_c	Average density of crystal assemblage	2700 kgm^{-3} [*Burgisser et al.*, 2010]	2550–3200 kgm^{-3}
ρ_m	Density of pure melt	2380 kgm^{-3} [*Burgisser et al.*, 2010]	
T	Magma temperature	1150 K [*Devine et al.*, 2003]	1100–1150 K
T_{diff}	Amount of cooling at conduit wall	200 K [*Collier and Neuberg*, 2006]	100–200 K
τ_s	Melt shear strength		10^5-10^7 Pa
$W_\%$	Initial dissolved water content of magma	4.5 wt% [*Barclay et al.*, 1998]	3–8 wt%
w, d, r	Variables that define the conduit shape and size	See Figure 4	See section 3.4.4

In order to assess the effect of altering the model parameters a standard or "reference" model is first defined. This reference model is based on data available in the literature that refers to Soufrière Hills Volcano, Montserrat, and is outlined in Figure 1 and Table 1. A detailed description of the parameters used in the reference model will follow in section 3.2, while we focus here on an outline of the modeling method. The dimensions of the modeled conduit shown in Figure 1 are inferred from geochemical and observational data from Soufrière Hills volcano [*Barclay et al.*, 1998, *Sparks et al.*, 2000], placing minimum depth constraints of 5–6 km below the surface for the position of the magma chamber and width estimates of 30–50 m for the conduit.

Figure 1. Cartoon of the modeled volcanic system. Bubble nucleation and brittle failure depth vary with the model parameters considered.

2.1. Governing Equations

Conduit flow is computed with a finite element approach, and modeled in an axial symmetric domain space through the compressible formulation of the Navier-Stokes equation:

$$\rho \frac{\partial \boldsymbol{u}}{\partial t} + \rho \boldsymbol{u} \cdot \nabla \boldsymbol{u} = -\nabla p + \nabla \cdot \left\{ \eta \left[\nabla \boldsymbol{u} + (\nabla \boldsymbol{u})^T \right] - \frac{2}{3} \eta [\nabla \cdot \boldsymbol{u}] \boldsymbol{I} \right\} + \boldsymbol{F}. \quad (1)$$

and the continuity equation:

$$\frac{\partial \rho}{\partial t} + \nabla \cdot (\rho \boldsymbol{u}) = 0 \quad (2)$$

where ρ is density, $\boldsymbol{u}$ the velocity vector, p the pressure, η the dynamic viscosity and $\boldsymbol{F}$ the volume force vector (gravity). There is no time dependency in the model and the terms $\rho \frac{\partial \boldsymbol{u}}{\partial t}$ and $\frac{\partial p}{\partial t}$ in equations (1) and (2) can be neglected.

2.2. Magma Composition

The properties of the magma are modeled as the averaged properties of its constituents: melt, crystals and gas. For the reference model, the general composition of the melt is taken as rhyolitic, using the

Table 2. Compositions of Melt Used in the Numerical Simulations

Composition[a]	SiO_2	Al_2O_3	TiO_2	FeO	MgO	MnO	CaO	Na_2O	K_2O
a	71.41	13.58	0.28	2.78	1.64	0.13	4.86	3.73	1.6
b	76.97	11.21	0.29	1.89	0.26	0.12	1.29	4.07	2.37
c	77.10	9.83	0.18	1.17	0.22	0.10	1.52	4.14	1.72
d	78.66	11.20	0.39	1.93	0.30	0.10	1.48	3.57	2.38

[a]Compositions determined through, (a) rastered electron microprobe analysis of groundmass [*Barclay et al.*, 1998]; (b) Matrix glass composition [*Rutherford and Devine*, 2003]; (c) Quartz hosted melt inclusion [*Devine et al.*, 1998]; (d) Cameca SX50 microprobe analysis of interstitial glass [*Burgisser et al.*, 2010]. All melts are rhyolitic and composition (a) is used in the defined reference model.

groundmass analysis of Montserrat dome rocks undertaken by *Barclay et al.* [1998]. However, several melt compositions, defined in Table 2 are ultimately considered to assess the effect of melt composition on the modeled eruption dynamics. Crystal content (χ_c) and density (ρ_c) are assumed fixed as we assume a constant temperature and that the conduit ascent times are orders of magnitudes faster than the time required for crystal growth by decompression, hence only the phenocrysts present in the magma chamber are accounted for and growth of microlites and microphenocrysts is not considered. The expression for the bulk density of the magma is given by

$$\rho = \rho_m \chi_m (1-\chi_g) + \rho_g \chi_g + \chi_c \rho_c (1-\chi_g),$$ (3)

where χ_m is the initial fraction of melt $(1-\chi_c)$, ρ_m is the melt density and χ_g is the gas volume fraction (Table 1). For the gas phase, water is assumed as the only volatile species present and the gas density (ρ_g) is calculated from the ideal gas law

$$pV = nRT,$$ (4)

where V is the volume of gas, R the ideal gas constant and T the temperature. The number of moles of water, n, is related to density by

$$n = \frac{M}{m},$$ (5)

where M is the molar mass of water and m is the mass of water present. Thus, combining (7) and (8) and considering a unit volume we get

$$\rho_g = \frac{mp}{RT}$$ (6)

In the reference model a single magma temperature is used with the exception of the temperature across a thermal boundary layer (TBL) defined adjacent to the conduit wall. A linear temperature drop is applied across the TBL, to simulate the cooling of the magma abutting the country rock in a well established conduit [*Collier and Neuberg*, 2006]. The gas volume fraction (χ_g) is calculated by determining how much water remains dissolved within the melt at a particular pressure using the solubility of H_2O in rhyolitic melts presented by *Liu et al.* [2005]. At high enough pressures, it is assumed that all the water is dissolved within the melt fraction and χ_g is initially zero, but as pressure decreases, water begins to exsolve out of the melt and forms bubbles. The absolute volume of exolved gas (V) can be calculated through rearranging the ideal gas law (4). This absolute volume of gas is then used to calculate the volume fraction of the bulk magma constituted by the gas phase.

2.3. Magma Viscosity

The bulk magma viscosity (η) is determined by first calculating the viscosity of the pure melt phase (η_m). This is done using a model for the viscosity of magmatic liquids presented by *Giordano et al.* [2008], that predicts the viscosity of silicate melts as a function of temperature and melt composition. It is important to note that the composition used in the viscosity model is that of the pure melt phase (rhyolitic) not the overall magma composition; the whole rock composition of recent Soufrière Hills Volcano magma is andesitic [*Edmonds et al.*, 2010], but this includes the contribution of the crystals. The viscosity model is only used to calculate the actual viscosity of the liquid component (the melt), on which the crystals (the solid) have no bearing. When the effect of crystals within the melt *is* considered, the effective viscosity of the melt (liquid) and crystal (solid) mixture (η_{mc}) increases, and can be represented by the Einstein-Roscoe equation

$$\eta_{mc} = \eta_m \left(1 - \frac{\chi_c}{\chi_c^{\max}}\right)^{-2.5}, \tag{7}$$

where $\chi_c^{\max}$ is the volume fraction of crystals at which the maximum packing is achieved [*Marsh*, 1981]. A commonly adopted value of $\chi_c^{\max} = 0.6$ [*Marsh*, 1981] is used within this study. Although this value was proposed for randomly packed spheres, and it has been shown by *Marti et al.* [2005] that $\chi_c^{\max}$ tends to decrease as the particle (crystal) shape becomes less isotropic, *Ishibashi* [2009] demonstrated that this value seems to be a good approximation as the effect of particle shape on $\chi_c^{\max}$ is offset by effects of size heterogeneity and crystal alignment.

The presence of bubbles also affects the viscosity. If the bubbles within the magma remain undeformed they act to increase η, but if they are deformed (elongated in the direction of flow), they act to decrease η [*Llewellin and Manga*, 2005]. Whether a bubble is in an undeformed or deformed state is represented by the capillary number

$$Ca = \frac{\eta_m r E}{\Gamma} \tag{8}$$

where r is the undeformed bubble radius, Γ, the bubble surface tension and E, a function of the strain rate within the magma flow defined below. If $Ca > 1$ then the bubbles can be considered deformed. Previous studies have calculated Ca as a function of only shear strain rate [e.g., *Pal*, 2003; *Collier and Neuberg*, 2006], of both shear strain rate and the rate of change of shear strain rate [e.g., *Llewellin and Manga*, 2005], or of shear strain rate and elongational strain rate [*Thomas and Neuberg*, 2012]. Here we adopt the approach of the latter. Bubbles can either be deformed though shear or extension, hence E can be defined as either the shear strain rate ($\partial v/\partial r$) or the elongational strain rate ($\partial v/\partial z$), with the rate that would have the greatest effect on bubble shape (largest value) being used to calculate Ca. To account for strain acceleration or deceleration the dynamic capillary number (Cd) is required [*Llewellin and Manga*, 2005]; this compares the time scale over which the bubbles can respond to changes in their strain environment with the time scale over which the strain environment changes. If this value is large, the flow is termed unsteady and the bubbles are unable to deform independently in response to the flow; they act in an unrelaxed, viscous manner, decreasing the relative viscosity of the suspension [*Llewellin and Manga*, 2005]. For the models considered within this study conditions of unsteady flow are found only in a very small area near the exit of the conduit. Accounting for this within the models resulted in no noticeable change in the derived flow parameters, hence the computation of Cd is not considered within this study.

Depending on the value of Ca, η is calculated using the suggested 'minimum variation' of *Llewellin and Manga* [2005]

$$Ca = \begin{cases} <1 & \eta = \eta_{mc}(1-\chi_g)^{-1} \\ >1 & \eta = \eta_{mc}(1-\chi_g)^{5/3} \end{cases} \tag{9}$$

By assuming the homogeneous nucleation of a number of bubbles in a unit volume of melt as a single event, which is determined from the initial bubble number density (b_{ni}) [*Hurwitz and Navon*, 1994], the bubble radius [*Lensky et al.*, 2002] is given by

$$r = \left[\frac{S_0^3 \rho_m (C_0 - C_m)}{\rho_g}\right]^{1/3}, \tag{10}$$

where C_0 and C_m are the initial and remaining amount of water dissolved in the melt respectively and S_0 is the initial size of the melt shell from which each bubble grows. S_0 is related to the instantaneous bubble number density (b_n) through the expression

$$S_0^3 = \frac{3}{4\pi b_n} \tag{11}$$

b_n is used rather than the initial value (b_{ni}) because since homogeneous nucleation is assumed, the bubble number density must remain constant with respect to the volume of the melt fraction in equation (3). This also accounts for bubble coalescence and b_n is given by

$$b_n = \frac{b_{ni}}{\chi_m}\left[\chi_m - \left(1 - \chi_g\right)\right] \tag{12}$$

2.4. Brittle Failure of Melt

It is now well established that magma, or more specifically the melt component of a magma can fail in a brittle manner [e.g., *Gotto*, 1999; *Neuberg et al.*, 2006; *Tuffen and Dingwell*, 2005; *Tuffen et al.*, 2008]. *Thomas and Neuberg* [2012] have also demonstrated that the generation of fracture zones at the conduit margins as a result of magma breakage can affect the overall conduit flow dynamics. This is because movement is likely to become concentrated along these fractures and offer reduced resistance to flow, resulting in increased flow velocities in these regions. In order to account for these effects it is necessary to define conditions under which the melt may fracture. Shear failure of melt occurs when the shear stress ($\eta\dot{\varepsilon}$) exceeds the shear strength (τ_s), and has been represented as the brittle failure criterion [*Tuffen et al.*, 2003; *Neuberg et al.*, 2006; *Okumura et al.*, 2010]

$$\frac{\eta\dot{\varepsilon}}{\tau_s} > 1 \tag{13}$$

where $\dot{\varepsilon}$ is the shear strain rate. This criterion holds true under the assumption that during unrelaxed deformation the accumulation of shear stress in the melt obeys the Maxwell model

$$\sigma_s = \frac{\eta}{\mu}\frac{\partial \sigma_s}{\partial t} = \eta\dot{\varepsilon} \tag{14}$$

where σ_s is the shear stress and μ the shear modulus.

2.5. Boundary Conditions

Flow within the system is driven by a pressure gradient defined by boundary conditions at the top and bottom of the conduit. The top boundary is set to atmospheric pressure at the altitude of the conduit exit plus any overburden load from an emplaced lava dome. The bottom boundary is set to lithostatic pressure (assuming a homogeneous country rock density of 2600 kgm^{-3}) plus any imposed overpressure (P_e). Both the top and bottom pressure conditions are held constant throughout the model run. Initial boundary conditions along the length of the conduit are defined as no slip. When brittle failure of melt is considered within a model run, in regions of the conduit wall where the brittle failure criterion was exceeded, the boundary conditions are changed to a tangential slip velocity ($\Delta\boldsymbol{u}$) defined by:

$$\Delta\boldsymbol{u} = \frac{1}{\beta}\sigma_s, \tag{15}$$

where σ_s is the tangential shear stress to the conduit wall and the coefficient β is a function of the slip length (L_s) which is defined as:

$$\beta = \frac{\eta}{L_s}, \tag{16}$$

The model is then rerun to account for the effect of changing boundary conditions at the conduit walls. Where this results in an increase in the predicted failure depth an iterative approach is used and the model is rerun with the new depth for the change in boundary conditions until the depth at which brittle failure of the melt stabilizes. For the purposes of this study the failure depth is considered to have converged if the depth increase between iterative runs is less than 10% of the previous observed increase.

3. Assessing the Sensitivity of Ascent Rate to Changes in Model Parameters

3.1. Magma Ascent Rates

The ascent rate is a key parameter in understanding volcanic hazard as it has been directly linked to eruptive behavior [*Gonnermann and Manga*, 2007; *Humphreys et al.*, 2008]. By gaining a better understanding of which model parameters have the greatest effect on ascent rates we can achieve an insight into which are the most important parameters that may control explosivity and the likely severity of the volcanic hazard.

The ascent rate has also been linked to monitoring data such as seismicity [e.g., *Thomas and Neuberg*, 2012] or deformation [e.g., *Zobin et al.*, 2011], so it is possible to link the changes in model parameters to recorded

monitoring data. In addition, there are physically observed variations in ascent rate estimated from a variety of methods ranging from studying mineral reaction rims around phenocrysts within erupted magma [*Rutherford and Devine*, 2003] to studying lava dome morphology [*Sparks et al.*, 2000]. This places constraints on the magnitude of changes to the modeled ascent rate engendered by altering the model input parameters we can consider realistic. Slow ascent rates can be inferred through observations made of extruding magma lobes at displacement rates of 20–30 md^{-1} [*Sparks et al.*, 2000], or approximately 2.5×10^{-4} ms^{-1}. Faster ascent rates have been calculated from quantifying the break down of hornblende in ascending magma by *Rutherford and Devine* [2003], these calculated rates ranged between 10^{-3} ms^{-1} to greater than 2.0×10^{-2} ms^{-1}. The value of 2.0×10^{-2} ms^{-1} obtained through this technique is however a minimum estimation of the maximum ascent rate as above this value the magma is thought to ascend quicker than the time it takes for the breakdown to occur, leading to an inability to calculate faster rates. This value representing a minimum is reinforced by observations of the growth of the lava dome at Soufrière Hills. Measurements of the lava dome volume from radar and photogrammetry have estimated the maximum observed extrusion rates to be ~ 20 m^{3}s^{-1} [*Ryan et al.*, 2010; *Wadge et al.*, 2010]. Achieving this extrusion rate from our reference model of a cylindrical conduit 30 m in diameter would require an ascent velocity of 3×10^{-2} ms^{-1}. These estimates, derived from both surface observations and petrological studies suggest that changes in ascent velocity of two orders of magnitude are commonplace.

Matching the absolute values of these observed and calculated ascent rates is currently beyond the scope of the model and this is discussed further in section 5. However we can use the magnitude of the observed variations to provide upper and lower bounds to the extent to which the model input parameters are varied. Any changes that produce increases in ascent rate greater than two orders of magnitude over the reference model are not considered realistic in this work. This may seem at first an arbitrary discrimination, but there is a good reason that the observed or calculated ascent rates presented in the literature [e.g., *Rutherford and Devine*, 2003; *Castro and Gardner*, 2008] are "slow" ($<5 \times 10^{-2}$ ms^{-1}). Accent rates faster than this, while likely to exist in nature, would almost certainly result in substantial fragmentation of the magma, making it very difficult to observe or calculate the actual magma ascent rate below the initial point of fragmentation. Fragmentation dynamics are not considered within the current model, hence no valid inferences or conclusions can be gained from studying the model runs that exhibit these fast ascent rates.

3.2. Defining the Reference Model
The results of the reference model provide the benchmark to which all other model runs will be compared. The most important element of the conduit model is the magma viscosity, and as discussed in section 2.3 this is calculated from three components: the melt, crystals and bubbles. A rhyolitic composition (Table 2) is used for the melt as this is the most commonly cited composition of the melt phase [e.g., *Devine et al.*, 1998; *Sparks et al.*, 2000; *Edmonds et al.*, 2010]. For the reference model the composition of *Barclay et al.* [1998] is used. This composition was chosen from those listed in Table 2 as it appears to be the least evolved, subsequent changes to the melt composition can then be made to assess the changes in an evolving magmatic system that may be expected after a sustained eruption period. The initial water content of the magma for the reference model was chosen as 4.5 wt%. This value was chosen as it derives from petrological evidence that defines the likely pressure conditions within the magma chamber [*Barclay et al.*, 1998, *Devine et al.*, 2003]. For magma of Soufrière Hills composition the glass density has been measured as 2380 ± 10 kgm^{-3} [*Burgisser et al.*, 2010] which is the value we adopt for the reference model. To calculate the viscosity of the melt a temperature is required. Many andesitic to rhyolitic eruptions, including those at Montserrat are thought to be triggered by the intrusion of hotter material into an existing magma chamber [*Murphy et al.*, 2000; *Snyder*, 2000], and there are several mineral phase stability studies that suggest both the long-term storage and maximum reheated temperature of the Soufrière Hills magma chamber prior to the onset of eruptive activity [e.g., *Barclay et al.*, 1998; *Devine et al.*, 1998; *Murphy et al.*, 2000; *Devine et al.*, 2003]. Consequently, based on these studies a temperature of 1150 K is chosen for the reference model representing the maximum inferred temperature at the start of the eruptive cycle. Using this temperature with the composition of *Barclay et al.* [1998] and an initial water content of 4.5 wt% yields a melt viscosity of 2.17×10^4 Pa.s from the viscosity model of *Giordano et al.* [2008]. However, as discussed in section 2.2 *Collier and Neuberg* [2006] showed that for a thin region adjacent to the conduit wall an isothermal assumption is not valid, and that for a cylindrical conduit of radius 15m, a cooling of 100–200 K can be expected over a thermal boundary layer (TBL) of 0.3–0.5 m. For this reason the reference model contains a TBL adjacent to

the conduit wall of 0.3 m thickness over which a liner 200 K cooling is applied. These values were chosen as it is assumed that the temperature difference between the magma and the surrounding country rock decreases with the longevity of the volcanic system, while the width of the TBL grows.

The crystal content of the reference model is based on petrological studies of the Soufrière Hills magma [e.g., *Barclay et al.*, 1998, *Murphy et al.*, 2000] and a value of 40%, at the lower range of those suggested (40–50%) is used as it is assumed that the crystal content would be at a minimum at the start of the eruption, increasing with time as the magma cooled. The crystal population mainly consists of plagioclase and pyroxene phenocrysts and the average crystal density of this population has been taken as 2700 kgm^{-3} [*Burgisser et al.*, 2010]. Estimates of bubble number densities range from 10^7 to 10^{17} m^{-3} [*Hurwitz and Navon*, 1994; *Lyakhovsky et al.*, 1996; *Cluzel et al.*, 2008; *Giachetti et al.*, 2010] while suggested values for the bubble surface tension range from 0.05 to 0.3 Nm^{-1} [*Lyakhovsky et al.*, 1996; *Llewellin et al.*, 2002; *Cluzel et al.*, 2008; *Ittai et al.*, 2011]. We can place some constraints on the bubble number density by considering the typical magma ascent rates discussed in section 3.1. At these ascent rates ($<5 \times 10^{-2}$ ms^{-1}) we can assume typical decompression rates of approximately 0.1–1 kPas^{-1}, and at these values *Cluzel et al.* [2008] demonstrated the bubble number density reaches a maximum of 10^{11} m^{-3} and a minimum of 10^7 m^{-3}. Incidentally, this minimum estimated value for the bubble number density was based on an absence of magnetite crystals, which were seen to act as preferential bubble nucleation sites. Magnetite is present in the Soufrière Hills magma [*Devine et al.*, 1998], so this low value is unlikely to represent normal conditions, hence a bubble number density of 10^{10} m^{-3} is used for the reference model. The range of values for bubble surface tension is not as large (Table 1), but it is harder to narrow down. The values depend on how hydrated the melt is, with the larger values being calculated for a dry melt. Our reference model has an initial water content of 4.5 wt%, hence we use a bubble surface tension of 0.06 Nm^{-1} representing the fact that the melt is not significantly dehydrated.

Low frequency seismic swarms are not the everyday observed activity at Soufrière Hills. Since it is this type of seismic activity that is thought to lead to the development of conduit margin fractures zones and viscosity controlled slip at the conduit walls [*Neuberg et al.*, 2006; *Thomas and Neuberg*, 2012] we do not include this in the reference model. Rather, the reference model is used to simulate conditions prior to brittle failure and the flow along the entire conduit length is modeled through no-slip boundary conditions. The reference model can then be built on to test individual parameters, one at a time, in order to assess how these parameters may drive the system to reach brittle failure and produce a detectable geophysical signal indicating changes in ascent rate.

The remaining two parameters we need to define are the pressure conditions at the bottom and top of the conduit that drive flow. For the reference model we assume there is no overpressure within the magma chamber, and the bottom pressure is set to lithostatic value at a depth of 4 km, assuming an average crustal density of 2680 kgm^{-3}. Correspondingly, for a conduit length of 5 km (Figure 1), the pressure at the conduit outlet is set to atmospheric pressure at a height equal to 1 km above sea level, representing the summit elevation.

3.3. The Reference Model Results
The results of the reference model to which all other models are compared are shown in Figure 2. Figure 2b shows seven vertical velocity profiles for depths below 1000 m that are spaced at 2.5 m from conduit centre, defined at 0 m, to the full conduit radius at 15 m. It can be seen that the peak ascent velocity occurs, as expected, in the centre of the conduit, with no slip boundary conditions at the conduit wall. At each 2.5 m increase away from the conduit centre the ascent velocity decreases. Figure 2c shows the ascent rate for a horizontal cross section through the conduit at a depth of 2500 m (the middepth of the model space). Integrating along this profile results in an average ascent velocity at this depth of 0.078 ms^{-1}. This is the same order of magnitude of ascent velocities as discussed in section 3.1. Integrating over the entire length of the vertical profile of ascent velocity in the conduit centre yields an average ascent velocity of 0.16 ms^{-1}. It is these two average velocities that will be used for comparison throughout this study, and will be referred to as the "total average ascent rate" ($\bar{V}$) and the "2500 m depth ascent rate" (V_{2500}). Averaged velocities are used as they provide a single point of comparison between models. They are also consistent with the observed/calculated values for ascent rates presented in section 3.1 which are based on either surface observations of dome extrusion turned into a single value for ascent rate assuming a cross sectional area
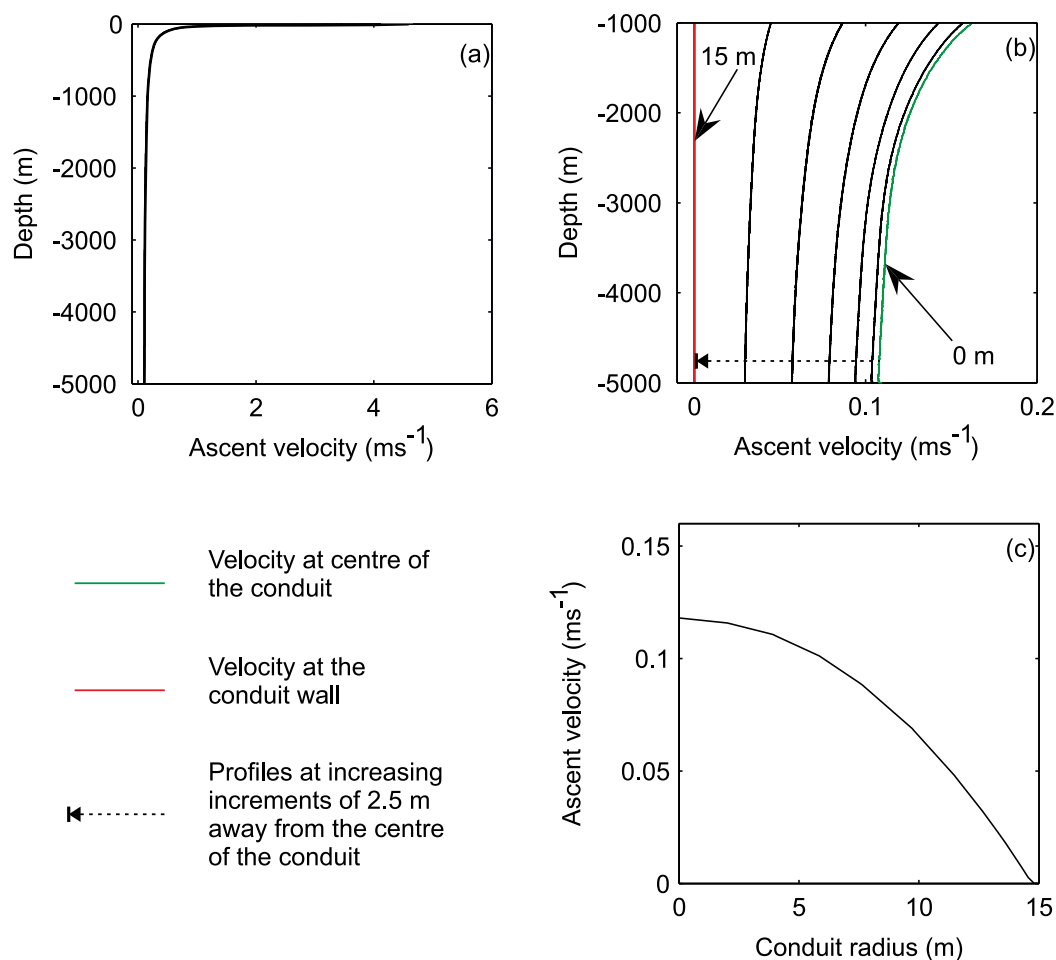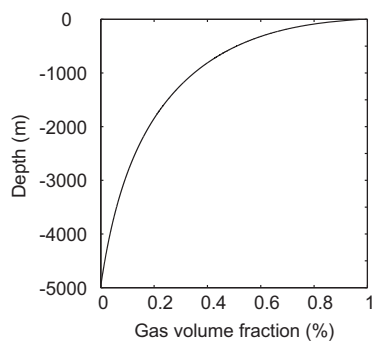
Figure 2. Ascent velocity calculated for the reference model. (a) Ascent velocity for a vertical profile through the centre of the conduit; (b) additional profiles at 2.5 m horizontal increments from the conduit centre to the conduit wall for depths greater than 1000 m; and (c) ascent velocity for a horizontal profile at a depth of 2500 m where 0 m is the centre of the conduit.

for the conduit, or a steady decompression rate calculated from mineral reaction rims turned into a corresponding single, average value for ascent rate.

We can place a good degree of confidence in the values of ascent velocity modeled below 1000 m as the gas volume fraction at this depth is calculated to be 35% (Figure 3). This corresponds to a similar value for the gas volume fraction proposed for the onset of permeable flow, suggested to control the start of significant permeable outgassing [*Candela*, 1991; *Rintoul and Torquato*, 1997]. Consequently, only above 1000 m depth does the gas volume fraction begin to increase markedly above what is likely if permeable outgassing was fully considered. As a result, the modeled magma properties below 1000 m are not significantly affected by slightly elevated volumes of exsolved gas, although the ascent velocity will be raised somewhat due to the requirement of mass conservation, meaning that the flow in this area will be faster than expected as it needs to keep up with the accelerated flow near the conduit exit. It is also worth noting that the reference model has been parameterized to represent the onset of eruptive activity (section 3.2), resulting in the magma temperature being at the top of the modeled range, and the crystal content being at the lower end of the modeled range (Table 1). These two end members of model parameters contrive a relatively low magma viscosity, which results in a relatively fast ascent velocity. With this in mind and the fact that the modeled values will be elevated due the lack of permeable outgassing, the calculated average ascent velocities of 0.078 ms^{-1} at a depth of 2500 m below the conduit exit and 0.16 ms^{-1} for the entire conduit length appear rational results, showing the reference model to be a reliable point of comparison with which to judge the effect of changing the model parameters.

Figure 3. Gas volume fraction (χ_g) for the reference model ($W_\% = 4.5$ wt.% H_2O; $P_e = 0$ MPa) versus depth.

3.4. Varying the Model Parameters

To gain an understanding of the relative importance of an individual parameter we first vary each separately (sections 3.4.1–3.4.5). However, as some parameters are intrinsically correlated to others we also model certain combinations of parameter changes in section 3.4.6

3.4.1. Magma Composition

All the published studies of Soufrière Hills magmas share the fact that the melt phase is described as rhyolitic [e.g., *Devine et al.*, 1998; *Sparks et al.*, 2000; *Edmonds et al.*, 2010]. However, this is a very broad classification and the precise composition can vary considerably (Table 2). In addition, the estimated water content of these magmas varies independently from ~ 4 wt.% [e.g., *Murphy et al.*, 2000] to theoretically greater than 10 wt.% when including the presence of a free gas phase [*Burgisser et al.*, 2010]. Although *Burgisser et al.* [2010] ultimately identified these extremely high total water contents as unlikely, they are included here to assess all possibilities. Therefore it is important to find out how significant these variations are to the modeled conduit flow dynamics. Hence we rerun the reference model with the changed magma compositions b, c, and d listed in Table 2, and we also run separate models with altered initial water contents of 2, 3, 6, and 8 wt.%. For these model runs it is assumed the composition and number of crystals/bubbles does not changes and this is considered separately in section 3.4.3. All results and comparisons of the various model runs can be found in section 4. Since the amount water dissolved in the melt is controlled by the solubility law of *Liu et al.* [2005], at the higher water contents the full amount of available water will not be dissolved in the melt at the depths considered. The excess will remain exsolved, and is present in the model as a free gas phase.

3.4.2. Temperature

There are three variables used in the model that relate to temperature. The first is the actual temperature of the magma, and the other two correspond to the cooling of the magma adjacent to the country rock in the Thermal Boundary Layer (TBL). Several different scenarios are modeled and compared to the reference results with T set to 1100, 1110, 1125, and 1140 K. However, the decrease in temperature (T_{diff}) and width of the TBL (D_{TBL}) have been constrained through previous work (Table 1) so only two model runs were completed in addition to the reference model for each of these variables, with T_{diff} and D_{TBL} being set to 150 and 100 K and 0.4 and 0.5 m, respectively. By varying T and T_{diff} independently we incorporate potential temperature changes in the confining edifice throughout the eruption history. Model runs where changes in these variables are linked are discussed in section 3.4.6.

3.4.3. Crystals and Bubbles

Although the crystals and bubbles are extremely small compared to size of the overall system they have a large effect on the overall flow properties since they are very efficient at modifying the viscosity of the combined fluid and particle suspension. Previous studies report differing crystal and/or bubble populations changing the bulk viscosity of the magma by two to eight orders of magnitude [e.g., *Llewellin et al.*, 2002; *Pal*, 2003; *Costa et al.*, 2009]. The crystal content discussed in section 3.2 has a fairly limited range, and accordingly models are run with crystal contents of 42, 45, 48, and 50% volume fraction. With the changes in crystal volume fraction the crystal assemblage may also change accordingly. The average density of the crystal assemblage (ρ_c) reported in Table 1 is based on the phenocryst population consisting of 15 vol% pyroxene and 85 vol% plagioclase [*Burgisser et al.*, 2010], hence to account for possible additions to, or changes in the relative proportions of the assemblage, the model is run using values for ρ_c of 2550, 2800, 3000 and 3200 kgm^{-3}.

Like the crystal content, the discussion in section 3.2 has also narrowed the range of values for the bubble number density (b_{ni}) and bubble surface tension (Γ) that we consider. Models are therefore run with values for b_{ni} of 10^7, 10^8, 10^9 and 10^{11} m^{-3} and values for Γ of 0.05, 0.1, 0.2 and 0.25 Nm^{-1}.

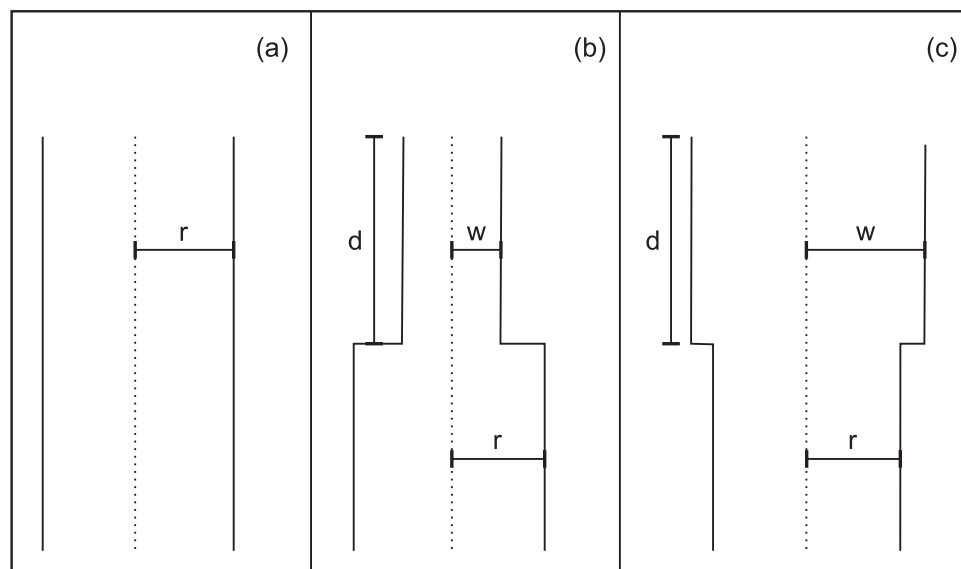#### 3.4.4. Conduit Geometry and Conditions Driving the Flow

During each individual simulation the pressure boundary conditions that act as the driving force for conduit flow are kept constant. However during the course of a long-lived silicic dome-forming eruption (such as

Figure 4. Schematic diagram of the alternative conduit geometries modeled, showing (a) a constant conduit radius; (b) a narrowing conduit; and (c) a widening conduit.

Soufrière Hills) it is entirely possible and indeed likely that the pressure within the magma chamber or at the conduit exit would alter due to factors such as fresh magma injection, or the increased overburden of a growing dome. To represent this fact we run several models with different boundary pressure conditions. To simulate increasing excess chamber pressure from fresh magma injection we run models with P_e set to 5, 10, 15 and 20 MPa and to simulate the suffocating effect of a growing lava dome we run models with P_{top} set to 2, 3, 4 and 4.5 MPa, where 4.5 MPa represents the overburden pressure of a 200 m high dome where the density of the dome rock is assumed to be 2250 kgm^{-3} [*Wadge et al.*, 2010].

Similarly to the probability of changing pressure conditions, it is likely that the conduit geometry might evolve over the course of a decadal eruption. Hence, for the purpose of this study possible conduit shapes were modeled, representing different conduit widths as well as the narrowing and widening of conduit sections. These are described as cases (a), (b) and (c) in Figure 4. Case (a) is the simplest geometry change and represents a simple change of the conduit radius (*r*). The reference model radius is 15m so to examine the effect of this parameter the model was also run with *r* equal to 10, 20, and 25 m. Case (b) represents a narrowing of the conduit, but the diameter of the shallow conduit is somewhat constrained by physical observations of spine width (section 2), consequently it was not reduced too far below the reference model radius of 15 m, and a single value for the reduced upper radius (*w*) of 10 m was used. To assess the impact of the depth of this change the reduction in the conduit radius is modeled at depths (*d*) of 1500 and 500 m below the conduit exit. Case (c) is similar to (b) but represents a widening of the conduit increasing the radius to 20 and 25 m and again, to assess the importance of the depth of this geometry change each increase in conduit radius was modeled at *d* of 1500 and 500 m below the conduit exit.

3.4.5. Brittle Failure of the Magma

All of the models previously described in section 3 assume simple laminar flow with no-slip boundary conditions and do not consider the brittle failure of the melt [e.g., *Gotto*, 1999; *Tuffen et al.*, 2003; *Neuberg et al.*, 2006]. *Thomas and Neuberg* [2012] demonstrated the importance of considering the brittle failure of melt as it can have a significant influence on the modeled flow dynamics. Brittle failure of melt has the potential to generate fracture zones adjacent to the conduit walls which allow the magma column to slip during ascent. First we include the brittle failure of melt in the model using values of 10^7 Pa for the melt strength and 0.1 m for the slip length [*Tuffen et al.*, 2003] to test how it changes the ascent rate against the reference model. Next we asses the importance of the melt strength and slip length using values between to 10^6 and 10^5 Pa, and 0.01, 0.5 and 1.0 m, respectively. These values reflect the reduced range of magma strengths expected due to the presence of crystals and bubbles [e.g., *Romano et al.*, 1996; *Okumura et al.*, 2010] and
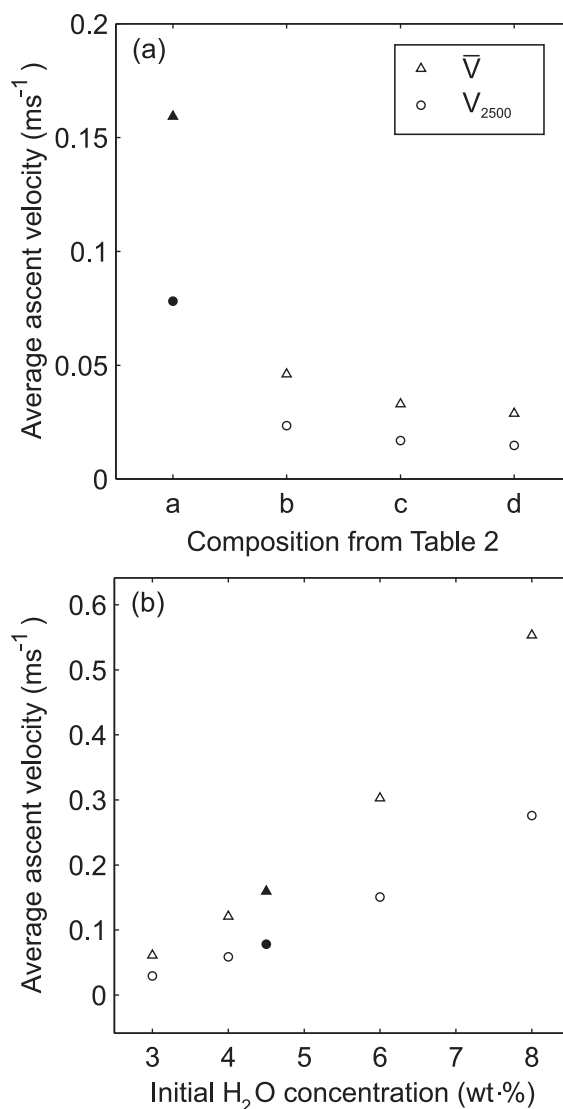
Figure 5. (a) Ascent velocities for models with different magma compositions and (b) initial water contents. The triangles represent values of the total average ascent rate ($\bar{V}$) and the circles represent values of the 2500 m depth ascent rate (V_{2500}). The filled symbols show the results of the reference model defined in section 3.2.

the range of fracture sizes observed in nature along conduit margins which determine the variation in the slip length [*Tuffen et al.*, 2003].

3.4.6. Changing Multiple Parameters

Rather than following a Monte Carlo approach and randomly vary all parameters within the defined ranges, which for solve time for each model and the number of variables altered would be computationally inhibitive, we focus on intrinsically linked parameters.

The temperature of the country rock may change due to conduction over an eruption period, but this happens slower than a temperature change of the magma, hence if magma temperature (T) changes, the difference between the two (T_{diff}) changes correspondingly. Also linked to magma temperature is crystallization; a higher degree of crystallization (i.e., larger values of crystal volume fraction (χ_c)) is achieved at lower temperatures. Therefore, we ran models with reduced values of both T and T_{diff} compared to those in section 3.4.2, and in addition with increased values of χ_c at lower temperatures.

The final pair of linked parameters that we consider is the melt strength (τ_s) and slip length (Ls). This relationship is based on the fact that if the melt is stronger, it requires a larger accumulation of shear stress to break it, and consequently, the rupture length will increase. Above the point of brittle failure this rupture becomes the length over which slip is considered in equation (15) and since the other terms in this equation are calculated, Ls plays an important role in scaling the rate of slip at the conduit walls.

4. Model Results

4.1. Effects of Changing Magma Composition

It is unsurprising that altering the magma composition has an effect on the modeled ascent velocity (Figure 5) for it is well known that the bulk composition of the melt is one of the main parameters which governs magma viscosity [e.g., *Bottinga and Weill*, 1972; *Shaw*, 1972; *Hui and Zhang*, 2007; *Giordano et al.*, 2008]. However, the four melt compositions modeled (Table 2) were all sourced from the analysis of Montserrat rocks, and all represented a rhyolitic melt, so significant changes due to the slightly different compositions were not expected. This is particularly true for the results presented in Figure 5a as the water content was taken to be a constant value of 4.5 wt.% for the purpose of testing these four compositions. However, the modeled total average ascent rate ranges from 0.03 to 0.16 ms^{-1} (Figure 5a). These may not seem like big absolute differences, but to put them in perspective, if we use these average ascent velocities to estimate the rise time of magma from the chamber to the surface within a 5000 m conduit it would range from
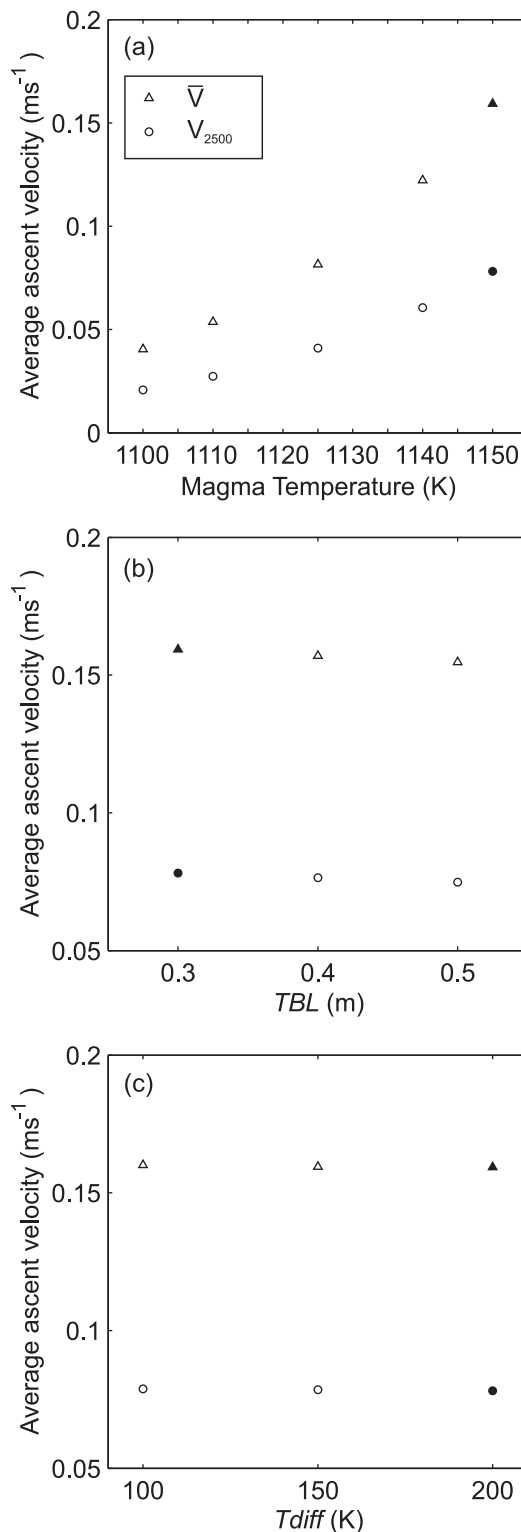
Figure 6. (a) Ascent velocities for models with different magma temperature (T); (b) thickness of the thermal boundary layer (D_{TBL}); and (c) temperature drop across the thermal boundary layer (T_{diff}). The triangles represent values of the total average ascent rate ($\bar{V}$) and the circles represent values of the 2500 m depth ascent rate (V_{2500}). The filled symbols show the results of the reference model defined in section 3.2.

approximately 2 days to 8.5 h. If we also consider the 2500 m depth ascent rate (Figure 5a) we see that the velocities span the value (2.0×10^{-2} ms^{-1}) highlighted by *Rutherford and Devine* [2003] that may indicate a transition from effusive to more explosive behavior. Remembering that all the melts modeled are classed as rhyolitic, these results show that it may be of vital importance to understand what the detailed makeup of the melt is rather than assuming a broad compositional average.

The initial dissolved water content of the melt is considered as the most important of the individual compositional controls on viscosity [*Vetere et al.*, 2008]. If we focus on this aspect of the melt composition it is easy to see why; changing this one parameter has a large effect (Figure 5b). In fact, altering only the initial dissolved water content causes larger changes in the ascent rate than changing all other components of the melt composition combined (Figure 5). The magnitude in the change of ascent rates caused by only altering the initial water content is approximately 10-fold, with the total average ascent rate ($\bar{V}$) ranging from 0.06 to 0.55 ms^{-1} compared to 0.16 ms^{-1} for the reference model (shown as in-filled symbols in Figure 5b). To use the previous supposition, this would result in estimated rise time differences from chamber to surface of approximately a day to 2.5 h. This is a clear demonstration of the importance of the initial water content in dictating the eruption dynamics.

It is noted that some of the modeled absolute ascent speeds presented appear very fast. The results are merely presented here with no further consideration, but discussion of the validity and meaning of the results follows in sections 4.7 and 5.

4.2. Effects of Changing Temperatures
Altering the three variables within the model that fall under the broad description of changing temperatures has a varying degree of effect. The result of changing these variables on the modeled ascent velocities can be seen in Figure 6. Changing the magma temperature has a considerable consequence on the modeled ascent rates, with $\bar{V}$ ranging between 0.04 and 0.16 ms^{-1} (Figure 6a). However, changing the variables that relate to cooling of the magma at the conduit
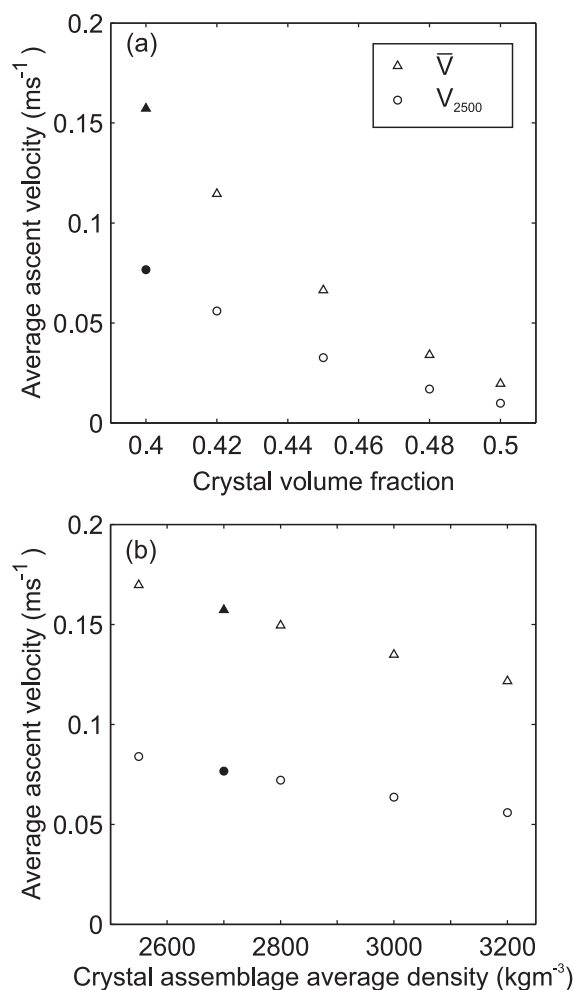
Figure 7. (a) Ascent velocities for models with different crystal volume fraction (χ_c). (b) Crystal assemblage average density (ρ_c). The triangles represent values of the total average ascent rate ($\bar{V}$) and the circles represent values of the 2500 m depth ascent rate V_{2500}. The filled symbols show the results of the reference model defined in section 3.2.

margins (D_{TBL} and T_{diff}) has a very minor direct influence. The largest deviation from the reference model of the total ascent rate (0.16 ms^{-1}) caused by altering either of these variables was only 5.0×10^{-3} ms^{-1} (Figures 6b and 6c). Although the magnitude of the effects may be different, all the changes are quite intuitive, lowering the magma temperature, higher degrees of cooling at the conduit margins and wider regions of cooling all result in lower ascent speeds.

4.3. Effects of Altering the Properties of the Crystal and Bubble Assemblages

First, let us examine the effect of crystals (Figure 7). By increasing the crystal volume fraction from the reference model value of 40–50%, $\bar{V}$ decreases from 0.16 to 0.02 ms^{-1} while the 2500 m depth ascent rate (V_{2500}) decreases from 0.078 to 0.01 ms^{-1} (Figure 7a). Both of these results hint at the importance of the amount of crystals in the magma and suggest that a 10% rise in the amount of crystals has the ability to cause a significant increase in the amount of time it takes the magma to rise to the surface. The results from changing the average density of the crystal assemblage present an interesting case (Figure 7b). In contrast to the results from changing almost all of the other model variables the change in ascent velocity with ρ_c is approximately linear. Furthermore, the difference between $\bar{V}$ and V_{2500} remains almost constant, rather than getting significantly smaller at slower ascent velocities. This suggests that compared to changing other variables, changing ρ_c equally effects the upper and lower conduit. The overall change in the modeled ascent velocities is also relatively small, with $\bar{V}$ varying between 0.157 and 0.170 ms^{-1}.

Changing the parameters in the model that relate to the bubbles does not have much effect on the ascent rate (Figure 8). Altering the bubble number density between 10^7 and 10^{11} decreases $\bar{V}$ from 0.163 to 0.155 ms^{-1}, with the greatest proportion of this decrease only occurring at the largest bubble number densities (Figure 8a). A similar behavior is seen for V_{2500}. Altering the bubble surface tension within the defined range has more of an impact (Figure 8b), with $\bar{V}$ ranging between 0.149 and 0.160 ms^{-1}, while V_{2500} ranges only between 0.073 and 0.079 ms^{-1}. Although altering the bubble surface tension has more of an effect than altering the bubble number density, the change from the reference model results of 0.16 ms^{-1} and 0.078 ms^{-1} for $\bar{V}$ and V_{2500} respectively are still small (Figure 8b). Similar to the results noted from changing ρ_c, the difference between $\bar{V}$ and V_{2500} remains fairly constant for changes in both the bubble number density and bubble surface tension, suggesting that changes in the properties of bubbles affects the upper and lower conduit equally.
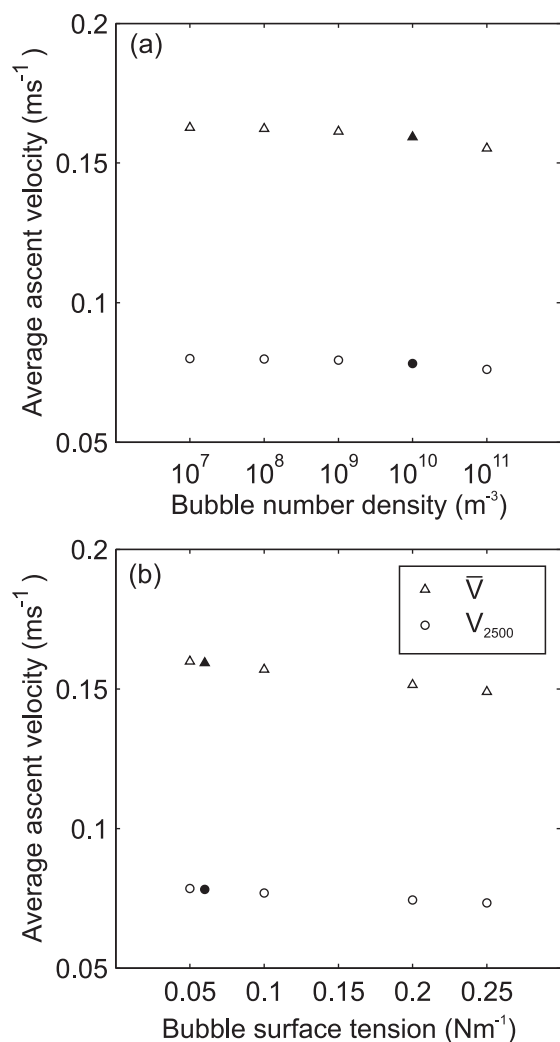
4.4. Effects of Changing the Conduit Geometry and Boundary Conditions

Changing the pressure gradient within the conduit (i.e., the driving force for the movement of magma) by altering either the top or bottom pressure had a marked effect on the modeled ascent dynamics. However,
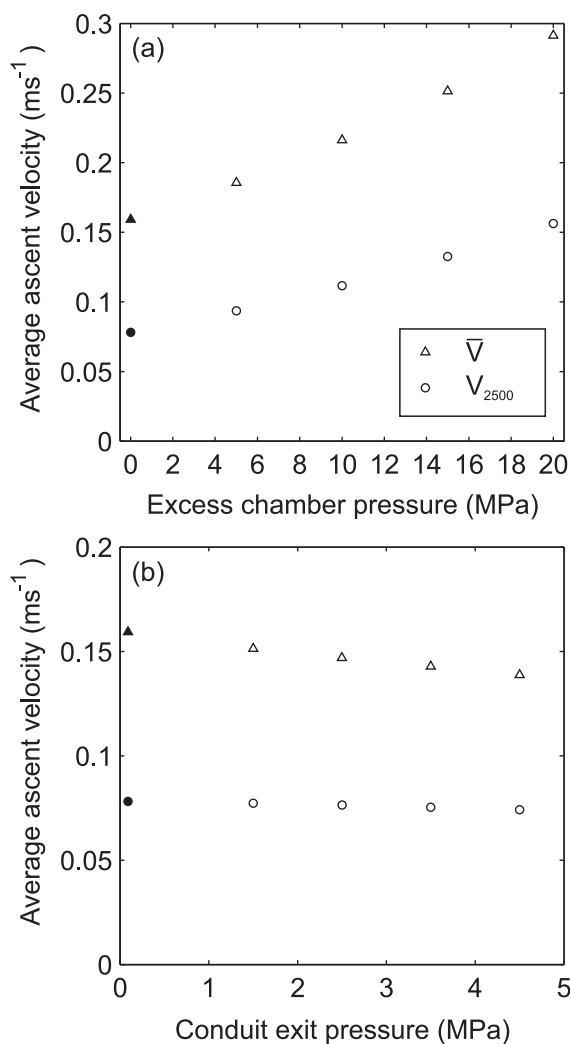
Figure 8. (a) Ascent velocities for different bubble number densities (b_{ni}). (b) Values of bubble surface tension (Γ). The triangles represent values of the total average ascent rate ($\bar{V}$) and the circles represent values of the 2500 m depth ascent rate (V_{2500}). The filled symbols show the results of the reference model defined in section 3.2.

for the range of parameters modeled the effect of altering the excess chamber pressure was greater than the effect for altering the confining pressure at the conduit exit (Figure 9). By increasing the excess chamber pressure from 0 to 20 MPa, $\bar{V}$ and V_{2500} increased from 0.16 to 0.29 ms^{-1} and 0.078 to 0.16 ms^{-1} respectively (Figure 9a). Conversely, by increasing the confining pressure at the conduit exit from atmospheric pressure to 4.5 MPa, $\bar{V}$ and V_{2500} decreased from 0.16 to 0.14 ms^{-1} and 0.078 to 0.074 ms^{-1} (Figure 9b), respectively.

How the geometry of the conduit could change over time is discussed further in section 4.7.1, but what is evident from the results of the conduit flow models is that the geometry of the conduit has a significant control on the modeled ascent dynamics. There were three different ways in which the conduit geometry was altered (Figure 4). However, the behavior of the flow was consistent in all three cases (Figure 10). When narrowing a part of, or the entire conduit with respect to the reference model the ascent velocity decreased, and when widening part or all of the conduit the ascent velocity increased. In detail, the relationship is a bit more complex and will be discussed in section 4.7. It is sufficient to note here that the slowest value of $\bar{V}$ of 0.061 ms^{-1} was caused by narrowing the upper part of the conduit to a radius of 10 m from a depth of 1500 m (Figure 10b) and the fastest $\bar{V}$ of 0.449 ms^{-1} was caused by widening the radius of the entire conduit to 25 m (Figure 10a).

4.5. Effects of Including Magma Fracture and Altering Magma Strength

The variation in ascent rates caused by including magma fracture in the models was surprisingly small, the total range of altered ascent rates caused by including this process and varying either the magma strength or slip length span only 7.67×10^{-6} ms^{-1} and 1.12×10^{-5} ms^{-1} for the V_{2500} and $\bar{V}$, respectively (Figure 11). In the reference model where slip was included using τ_s of 10^7 Pa and L_s of 0.1 m, failure was initially observed at a depth of 29 m. As described in section 2.4, if brittle failure was observed in a model, the boundary conditions were changed from that observed depth upward to include slip and the model was rerun with the new boundary conditions. This process was then repeated until the observed depth of brittle failure stabilized. The biggest increase in depth of brittle failure was seen when using τ_s of 10^5 Pa; causing an increase in the observed depth of failure from 29 to 504 m. This model run also produced the greatest increase in ascent velocities resulting from the inclusion of the brittle failure of melt (Figure 11), and when compared to the results from changing the slip length to larger values (Figure 11) suggest that it is the length of the conduit over which slip can occur that has the greatest effect on ascent rates rather than the absolute distance of slip. We note that the effect on the average ascent rates are small because two different flow regimes counteract each other above and below the depth of brittle failure. Overall by considering slip at the conduit walls it becomes easier to move material through the conduit and the volumetric

Figure 9. (a) Ascent velocities for models with different excess chamber pressure (P_e) and (b) conduit exit pressure (P_{top}). The triangles represent values of the total average ascent rate ($\bar{V}$) and the circles represent values of the 2500 m depth ascent rate V_{2500}. The filled symbols show the results of the reference model defined in section 3.2.

throughput of magma increases. While no-slip boundary conditions maintain a near parabolic flow profile, causing an increase in the ascent velocity in the centre of the conduit, the slip conditions above the brittle failure depth lead to plug flow, with a reduced velocity in the centre of the conduit.

4.6. Effects of Changing Multiple Parameters

The effects of altering the magma strength and slip length simultaneously seem to have a minimal additional effect on the average ascent rates compared to alter each individually. However, if one considers the flow conditions below and above the brittle failure depth separately (see above) it becomes obvious how the different behavior of parabolic and plug flow counteract each other as both flows are linked by the conservation of mass. We will discuss this complex behavior together with the influence of conduit geometry in more detail in section 5.3.

Altering the magma temperature in conjunction with changing the temperature decrease across the thermal boundary layer has little impact compared to altering just the temperature, with the largest difference caused by altering both parameters rather than just the magma temperature. This results in decreases of 1.2×10^{-3} ms^{-1} for $\bar{V}$ and 9.0×10^{-4} ms^{-1} for V_{2500}. Both of these maximum differences represent an increase in the ascent velocities caused by decreasing the magnitude of the temperature drop (from 200 to 100 K) across the TBL and occur at the highest modeled magma temperatures (Figure 12). This is because the effect

of decreasing the temperature drop across the thin layer (Figure 6c) is insignificant compared with the effect of a bulk temperature decrease (Figure 6a) and the resultant average ascent velocities are similar to those reported in section 4.2 for simply changing the magma temperature. In stark contrast, through conceptually linking a drop in magma temperature with enhanced crystallization, the effect of jointly altering T, D_{TBL}, and crystal content has a large effect on the modeled ascent rates (Figure 12 insets). The majority of this change can be attributed to altering the magma temperature and crystal content, and by increasing the crystal fraction content to 50% at a temperature of 1100 K in conjunction with a D_{TBL} decrease of 100 K, the modeled ascent rates drop by an order of magnitude from 0.04 to 0.005 ms^{-1} (Figure 12b) and 0.02 to 0.003 ms^{-1} (Figure 12a) for $\bar{V}$ and V_{2500} respectively. This suggests that any potential linkage between magma temperature and magma crystal content is very important.

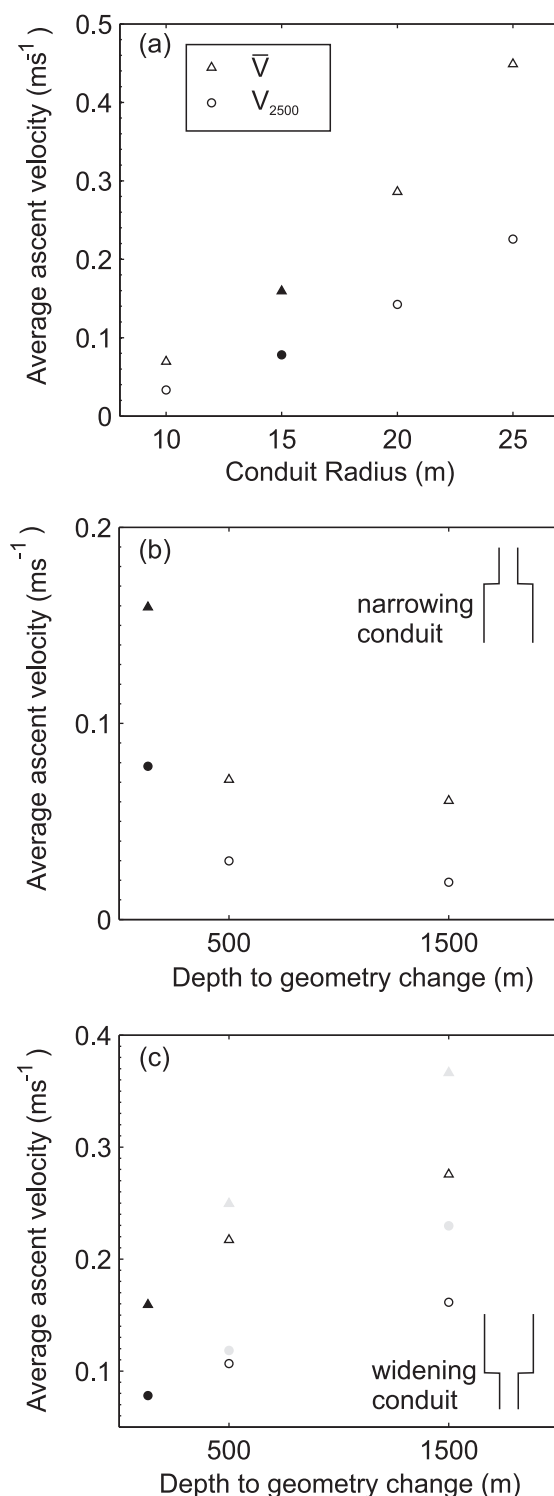### 4.7. Comparing the Relative Importance of Chosen Model Parameters

Figures 13 summarizes the sensitivity of ascent rates to different parameters. The single parameter (within the modeled ranges) which has the strongest effect on the ascent velocities is the initial dissolved water content of the magma. This parameter affected both $\bar{V}$ and V_{2500} to a large degree. In contrast there are several model parameters which have little effect on the modeled ascent velocities. These include the thermal

Figure 10. Ascent velocities for different conduit geometries. (a) straight conduit with variations in radius (*r*), (b) a narrowing conduit with reduced upper radius (*w*) of 10 m, and (c) a widening conduit with increased upper radius (*w*) of 20 m (open symbols) and 25 m (light filled symbols). The triangles represent values of the total average ascent rate ($\bar{V}$) and the circles represent values of the 2500 m depth ascent rate (V_{2500}). The dark filled symbols show the results of the reference model defined in section 3.2.

boundary layer thickness and the temperature drop across it, as well as the bubble number density and bubble surface tension. Modifying the parameters involved in the brittle failure of the melt (magma shear strength and slip length) (section 4.5, Figure 11) has a negligible effect on ascent rates and these results have not been plotted on Figure 13. However, their impact on the flow dynamics is very interesting and will be discussed in section 5.3.

It is unsurprising that the group of model parameters that appear to have the greatest effect on the magma ascent velocity as seen in Figure 13 (water content, temperature, crystal content, and chemical composition) also have the greatest effect on the magma viscosity. Ultimately, modeling the ascent of magma is a fluid flow problem, and the properties that have the biggest effect on the fluid (magma) properties will have the biggest effect on the overall dynamics of the system. All other parameters have a much smaller direct effect on the fluid properties, and although if considered in isolation may be important to specific small scale magmatic processes, in respect to magma ascent they are less important. For example by altering the properties of the bubbles within the magma, b_{ni} and Γ, the effect is to change the shape and number of bubbles in the magma, but their effect on the overall flow is minimal (Figure 13). It appears that it is the total volatile content (water in this case) which is available that is more important than how exactly it is stored in the magma.

4.7.1. Volatile Content and Pressure

The water, or in general the volatile content in a magma controls two mechanisms of altering ascent rate. (i) The ascent rate is increased as there is a larger amount of water dissolved within the melt; reducing the magma viscosity. (ii) The increased water content leads to more exsolved volatiles causing the density of the magma to decrease, increasing buoyancy. Both of these mechanisms will influence ascent rate with increasing volatile content.

These two effects are manipulated in opposite ways by the total pressure in the magmatic system, which through the solubility law, controls both the amount of *dissolved*
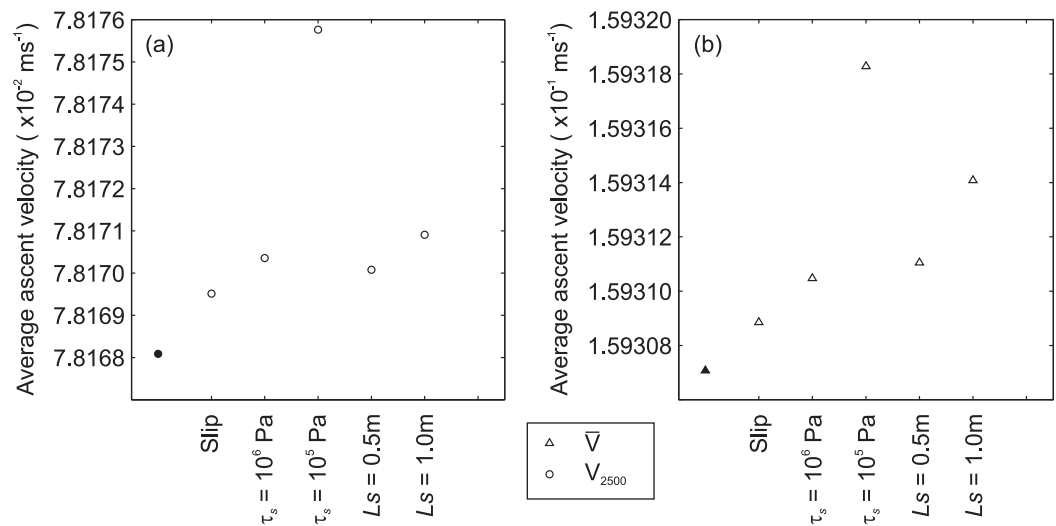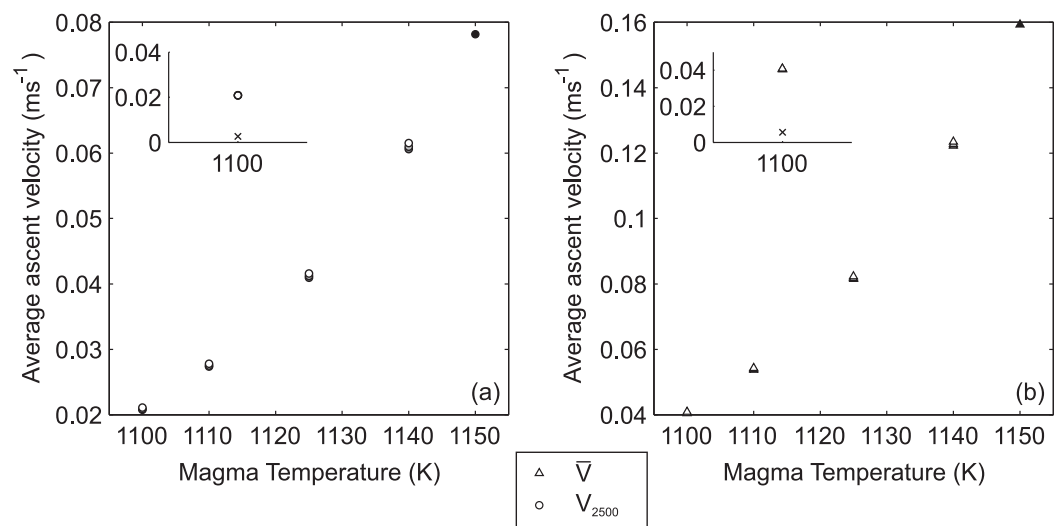
Figure 11. Plots of (a) the 2500 m depth ascent rate and (b) the total average ascent rate for models where brittle failure of the melt is considered, Ls is the slip length and τ_s the melt shear strength. The filled symbols show the results of the reference model defined in section 3.2. The results of altering Ls to 0.01 m are not plotted as it did not noticeably alter the results of the reference model.

volatiles affecting viscosity and the amount of *exsolved* gas available to drive buoyancy. The effect of increasing the excess pressure in the chamber (P_e) is presented in Figure 14 where plots of $\bar{V}$ for models with initial water contents of 3, 4.5 and 8 wt.% are shown for differing values of P_e. Although the total increase in P_e is the same for all three models (5–20 MPa), there is a much larger increase in the modeled velocity for the case of an initial water content value of 8 wt.%. Compared to changes in the driving pressure, the volatile content is seen to dominate the ascent rate. This reinforces the importance of the total volatile content in magma to conduit flow dynamics.

4.7.2. Bottom-Up or Top-Down Control
All of the results discussed so far in section 4.7.1 relate to changes caused by variations in parameters that would likely originate in the chamber region or deep in the conduit, but can shallower processes also significantly affect the conduit flow dynamics? The two parameters we examine here that represent potential

Figure 12. Plots of (a) the 2500 m depth ascent rate and (b) the total average ascent rate for models where the magma temperature (T) and amount of cooling at the conduit wall (T_{diff}) are both altered. The black, gray and open symbols represent T_{diff} values of 200 K, 150 K, and 100 K, respectively. The inset shows the decrease in the ascent velocities caused by altering the crystal volume fraction (χ_c) to 0.5 (cross) in a model where $T = 1100$ K and $T_{diff} = 100$ K.
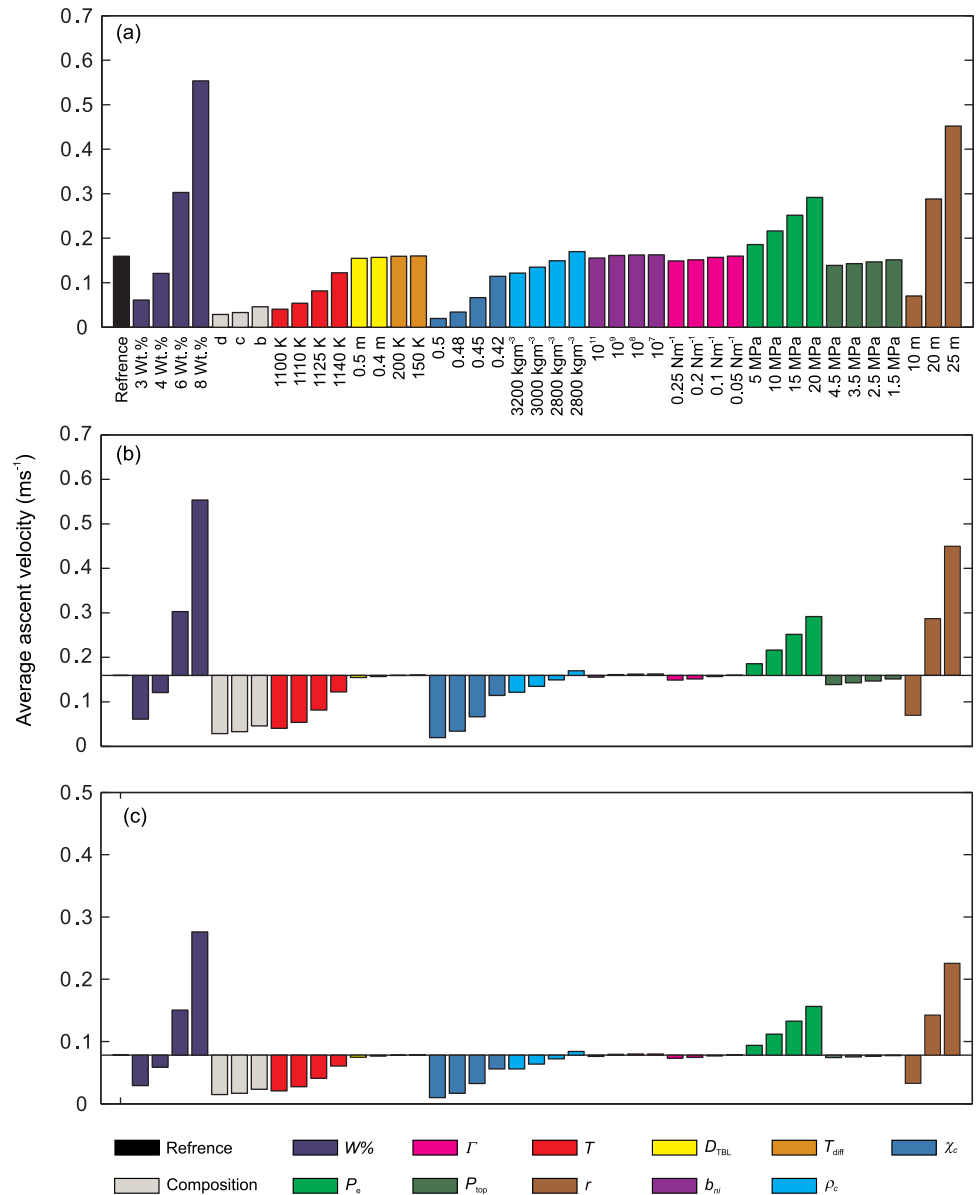
Figure 13. (a) The total average ascent rate (V̄) for each value of the parameters altered. The black bar represents the reference model with parameters as listed in Table 1. (b) The same data as Figure 13a plotted relative to the reference model, which is represented by the horizontal black line. Parameter changes that caused increases in the ascent rates plot upward from the horizontal line, while parameter changes that caused decreases in ascent rates plot downward. (c) The 2500 m depth ascent rate (V_{2500}) for each value of the parameters altered, plotted relative to the reference model.

shallow controls are P_{top} and the alterations in the conduit geometry (as we only consider changes in the top 500 m). As discussed in section 3.4.4 it is likely that either of these parameters might change over a long running eruption so it is important to see how changes could affect the flow dynamics.

With the exception of a few studies [e.g., *de' Michieli Vitturi et al.*, 2008, 2010] the effect of an evolving conduit geometry on the basic dynamics of conduit flow remains largely unexplored. The results presented here show that it is in fact a very important controlling mechanism, and only small changes in geometry cause large change in the modeled ascent rates, with the magnitude of these changes second only to altering the initial dissolved water content (Figure 13). If we look at the role of P_{top}, we find that the effect of altering it is not as great as altering other parameters, but we note that there is a relatively greater effect on V̄ (Figure 13b) than on V_{2500} (Figure 13c). This suggests that this parameter has a greater control on the upper part of the conduit than the lower. While the changes are relatively small, this may make it a very important parameter
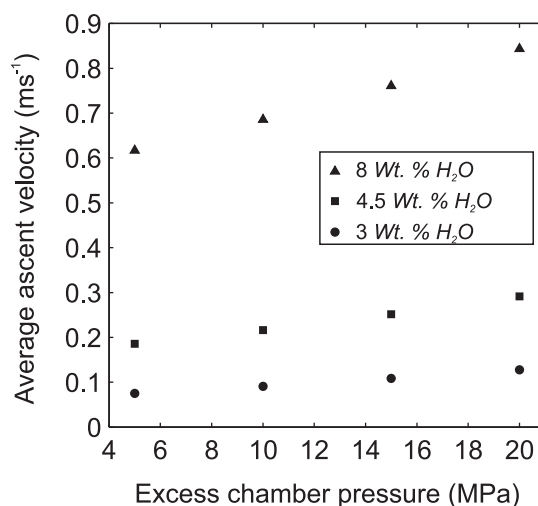
Figure 14. Total average ascent rate ($\bar{V}$) verses excess chamber pressure (P_e) for models with differing initial water content ($W_\%$).

as ultimately it is the behavior of the system in the upper parts of the conduit that dictates the eruption style. In summary, the results presented here suggest that shallow changes have the ability to significantly affect the system (particularly changes in the shallow conduit geometry). The notion of such a shallow control on eruption dynamics is not commonly thought of, and changes in the eruptive behavior of a volcanic system are almost always linked to changes at depth. However, it appears possible that some changes in volcanic activity may indeed be driven by top-down controls.

Finally we like to mention here the role of permeable outgassing and the presence of a free gas phase as an additional top-down control. A free gas phase (exsolved bubbles) has been shown to have an important control on ascent rates, but the amount of free gas present within the system will be determined by degassing mechanisms. Significant gas loss is likely to occur only in the upper region of the conduit, where sufficient pathways for permeable outgassing may be present. Therefore, the ability of the system to store or loose gas is seen as an additional important factor in the potential top-down control of magma ascent dynamics.

5. Limits of the Model

When trying to model such a complex, interdependent system, it is impossible to try and model every possible process, and given realistic time and computing power constraints there will always be some limitations in any model of a volcanic system. Here we have developed a model that looks at a wide range of processes and values of individual parameters that represent those processes, all controlling the ascent rate of magma within an established conduit system. How these parameters affect the flow dynamics and their relative importance has been discussed, however, there are some notable omissions that could affect any conclusions drawn, and they are discussed in detail below.

5.1. Independent Bubble Rise, Bubble Growth, and Permeable Outgassing

While it is noted in the introduction that the results presented have applicability to all volcanic systems, the degree of relevance to basaltic systems may be limited. In low-viscosity mafic systems bubbles are known to rise independently of the melt phase [*Gonnermann and Manga*, 2007]; a process not reflected in the current model. This process has been suggested as a potential contributor to the style of basaltic eruptions [e.g., *Del Bello et al.*, 2012], hence to fully understand the behavior of low-viscosity mafic systems it needs to be considered in the future. An additional aspect of bubble behavior that is imperfect in the current model is bubble growth. All current bubble growth is considered as occurring under equilibrium conditions and the effect of viscous resistance to bubble growth [e.g., *Melnik et al.*, 2005; *Gonnermann and Manga*, 2007] is not taken into account. This means that overpressures are not developed within the bubbles and the possibility of fragmentation occurring in response to exceeding a critical overpressure is not reflected. If such a process were to occur it would drastically alter the flow dynamics within the model.

The most obvious omission from the model is shallow gas loss from the system, a ubiquitous occurrence at any volcano, underpinning most volcanic activity [*Oppenheimer et al.*, 2003]. It is therefore important to understand how the inclusion of this process may affect the results of the models previously discussed. Since independent bubble rise is not implemented in the current model the discussion here relates only to gas lost via permeable flow. Figure 15 compares the results of the reference model to the results from a model with "forced" permeable outgassing, where gas loss is replicated by instigating an empirical permeability depth profile. No permeable outgassing of the system is imposed below 2000 m, corresponding to a porosity of 20% in the reference model (Figure 3). This depth was chosen as a compromise between the
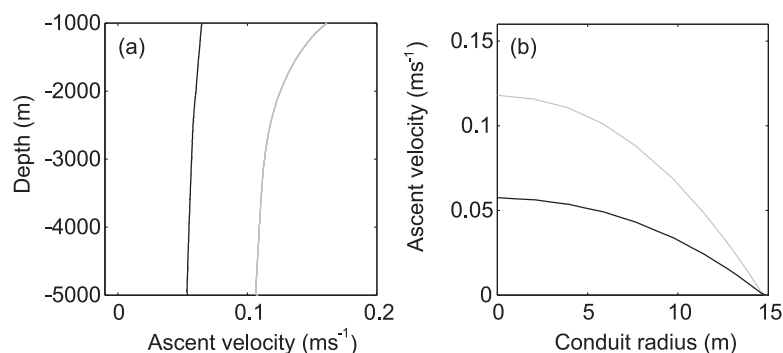
Figure 15. Plots of the difference in ascent velocity between the reference model (gray line) and a degassed model (black line), (a) for a vertical profile through the centre of the conduit and for depths greater than 1000 m and (b) for a horizontal profile at a depth of 2500 m.

theory that a porosity threshold is required at which permeable gas flow commences, commonly cited as 30% [e.g., *Candela*, 1991; *Rintoul and Torquato*, 1997], but up to as high as $\geq 70\%$ for crystal-poor silicic pumice [*Rust and Cashman*, 2011] and works by authors such as *Mueller et al.* [2005]; *Taddeucci et al.* [2006]; and *Okumura et al.* [2010] which indicate that significant permeability can develop via other mechanisms at low total porosity values (even $<30\%$). Above this depth it is assumed that permeable gas flow is established and a variable amount of the exsolved volatile is lost from the system following a linear gradient ranging from 0% loss at a depth of 2000 m to 95% loss at the conduit top (0 m). This mimics the effect of increasing permeability with decreasing depth (more gas is lost at shallower levels due to the higher developed permeability) and the value of 95% was chosen as it resulted in a good approximation of the upper value of preexplosive porosity of Montserrat rocks (50–60% vol.) [*Giachetti et al.*, 2010].

The results show that the effect of permeable outgassing on the magma ascent dynamics is significant, and although the magma is only assumed to degas at shallow levels (depths of less than 2000 m) the ascent dynamics of the entire conduit are altered. The ascent velocity is seen to be markedly reduced along the entire length of the conduit (Figure 15a), and there is a clear decrease in the cross-sectional profile of ascent velocity at a depth of 2500 m (Figure 15b), which is significantly below the depth at which permeable outgassing is implemented. This is mainly due to a feedback effect of increasing the viscosity at depths <2000 m due to the loss of the gas phase. This increases the overall flow resistance of the entire magma column since it is more difficult to extrude the more viscous magma, which acts as a plug. Consequently, if the driving forces behind magma flow remain constant the ascent velocity will decrease. It is because of this change in the entire ascent velocity profile that permeable outgassing is discussed as a potentially important top-down control on conduit ascent dynamics in the previous section. It is also worth noting that by reducing the gas volume fraction through permeable outgassing the ascent velocities are also reduced to a level that matches the magnitudes of the observed rates ($10^{-3}-10^{-2}$ ms^{-1}) discussed in section 3.1. This indicates that permeable outgassing plays an important role in determining the absolute ascent rates.

These results raise the question of how much we can reliably conclude from the models previously discussed where no permeable outgassing is considered. The results plotted in Figure 16 and presented in Table 3 show a comparison for a sweep of three different variables (excess chamber pressure, crystal volume fraction and initial H$_2$O content) for a degassed conduit versus a nondegassed conduit. Simulating the permeable outgassing of the magma is observed to have a significant effect, and both $\bar{V}$ and V_{2500} are reduced in the degassed models (Figure 16). However, the relative changes caused by altering the model parameters in both $\bar{V}$ and V_{2500} are very similar for the degassed model and the model where permeable outgassing is not considered (Table 3). While the model presented for permeable outgassing is a simple one and there are more complex solutions in existence [e.g., *Gonnermann and Manga*, 2007; *Ida*, 2007], the aim was not to accurately model gas flow, which no model currently does, but to the examine the broad effects of gas loss. The implemented model does this and the results suggests while gas loss may act to globally slow magma ascent, potentially causing changes to the secondary processes that occur within the conduit, the general overall effect of changing the model parameters on the ascent dynamics are the same whether permeable outgassing is considered or not. Consequently, although the results presented in section 4 overestimate the ascent rate, the processes that determine relative changes in magma ascent velocity
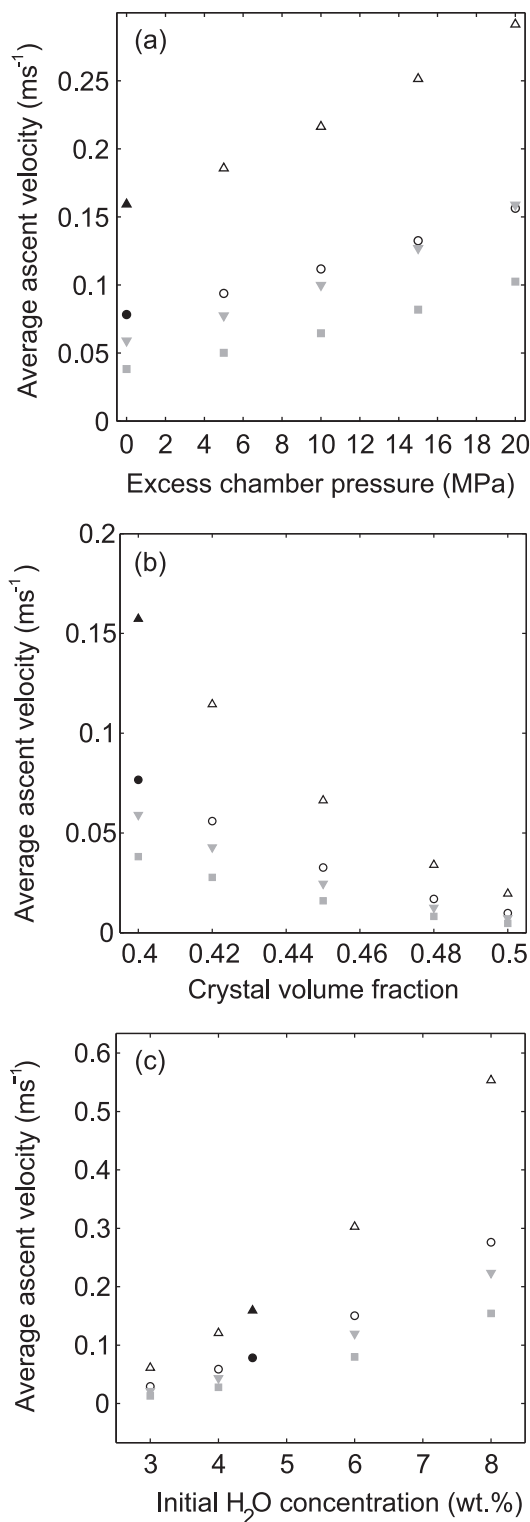
Figure 16. Ascent velocities for models with different values of (a) excess chamber pressure (P_e); (b) crystal volume fraction (χ_c); and (c) initial dissolved water content ($W_\%$). The triangles represent values of the total average ($\bar{V}$) ascent rate and the circles represent values of the 2500 m depth ascent rate (V_{2500}). Open symbols represent nondegassed models and gray symbols represent models where permeable outgassing was simulated. The dark filled symbols show the results of the reference model defined in section 3.2.

remain valid, and we can still use the models to assess the relative importance of individual model parameters.

5.2. Cooling and Decompression Induced Crystallization

As described in section 2.2 the crystal content is kept fixed within each individual model run as we assume a constant temperature and that the conduit ascent times are orders of magnitudes faster than the time required for crystal growth by decompression. This is an assumption made for ease of modeling, and reported crystal growth rates of $10^{-8}-10^{-12}$ ms^{-1} for hydrous felsic systems in response to multistep and single-step decompressions [*Hammer*, 2008] compared to the calculated average ascent rates of 10^{-3} (considering degassing) to 10^{-1} ms^{-1} support this assumption. However, the results presented in section 4.6 suggest that any linkage between decreases in temperature and increases in crystal content could be very significant. In addition *Sparks et al.* [2000] indicated that crystallization of microlites within the magma due to decompression during ascent may also play an important role. Hence, crystal and microlite growth will be considered in future developments of our model to include processes with longer time scales.

5.3. The "Real" Effect of Brittle Failure

As presented in section 4.5 the depth at which the models presented in this study predict the fracture of magma is shallow; < 500 m. At this depth the viscosity of the magma is very high and the slip velocity (equation (15)) is correspondingly low. However, the location of low-frequency earthquakes, thought to be the geophysical signals produced by the fracture of melt are observed at Montserrat to occur at much deeper levels [*Neuberg et al.*, 2006]. This is a problem addressed by *Thomas and Neuberg* [2012], who found that by altering the conduit geometry it is possible to cause fracture of the melt at deeper levels. This is because changes in the conduit geometry along its length cause divergence or convergence of the flow field within the conduit. This produces increases in the shear strain rate, and ultimately an increase in the shear stress

Table 3. Sensitivity Analysis of Ascent Rate for Degassed and Nondegassed Models

Model parameter	Total Average Ascent Rate ($\bar{V}$)		
	Min. Value (ms^{-1})	Max Value (ms^{-1})	% Change
P_e	0.157	0.291	85
P_e*[a]	0.059	0.159	169
χ_c	0.020	0.157	685
χ_c*[a]	0.007	0.059	742
$W_\%$	0.061	0.553	806
$W_\%$*[a]	0.021	0.223	961
	2500 m depth ascent rate (V_{2500})		
Model parameter	Min. Value (ms^{-1})	Max Value (ms^{-1})	% Change
P_e	0.078	0.156	100
P_e*[a]	0.038	0.102	168
χ_c	0.010	0.078	680
χ_c*[a]	0.005	0.038	660
$W_\%$	0.029	0.276	851
$W_\%$*[a]	0.013	0.154	1084

[a]Results from a degassed model.

(equation (14)) accumulated within the magma. Work by other authors [e.g., *Costa et al.*, 2007; *Hautmann et al.*, 2009] suggest a significant change in geometry at a depth of approximately 1500 m below the dome. Assuming that this change in geometry is able to cause locally high enough stresses to fracture the magma, this means that now a larger conduit section experiences a lower flow resistance as a result of slip conditions at the conduit walls above the brittle failure depth, accelerating the extrusion rate. If we apply the slip boundary conditions discussed in section 2.5 from a depth of 1500 m with a slip length of 0.1 m the total average ascent rate increases to 0.23 ms^{-1}. Compared to the reference model total average ascent rate of 0.16 ms^{-1} this is a significant increase and demonstrates the potential of the generation of fracture zones at the conduit walls to alter the overall conduit flow dynamics.

Another consideration concerns possible reductions in the viscosity term used in the calculation of the slip velocity in equation (15). We assume the viscosity of the magma as the viscosity of the slip surface. The slip surface may be lubricated by escaping volatiles leading to a reduction in the apparent viscosity of the slip surface and a further reduction in the flow resistance. The overall acceleration of magma extrusion due to a reduction in the resistance to flow at the conduit walls could also explain the accelerating behavior of earthquake swarms recorded at Montserrat [e.g., *Hammer and Neuberg*, 2009]. However, it should be noted that the effect of brittle failure might be reduced by the potential healing of the fractures [e.g., *Yoshimura and Nakamura*, 2010] not considered in this study, or by the lowering of the magma viscosity via shear heating at the conduit margins, reducing the shear stress accumulation (equation (14)). The relative importance of shear heating in mitigating brittle failure of the melt can be characterized by a Brinkman Number [e.g., *Gonnermann and Manga*, 2007]. However, for this study shear heating is not included as we assume that brittle failure of the melt is ultimately achieved; being considered the source process of the of low frequency seismicity observed at silicic volcanoes [e.g., *Gotto*, 1999; *Tuffen et al.*, 2003; *Neuberg et al.*, 2006; *Thomas and Neuberg*, 2012].

6. Implications for Volcanic Conduit Modeling and Volcano Monitoring

With never ending increases in computing power and the growing availability of user-friendly modeling software there is a mounting tendency for numerical models within the geosciences to grow ever more complex. Volcanology is not immune to this trend, but the results presented here show that it is sometimes the most basic model parameters, which appear to affect the whole system to the greatest degree. In particular the water content of the magma has been shown here to be a very important factor, and this mostly likely extends to other volatile species not considered. Yet it is very difficult to say how, why, or when this parameter may change during an extended period of volcanic unrest or eruptive activity. For example, even in a theoretically simple case of small volume; mafic; monogenetic volcanism, where one may expect the single pulse of erupted magma to be reasonably homogeneous, melt volatile contents have been shown as highly variable [e.g., *Johnson et al.*, 2010]. In cases such as this *Johnson et al.* [2010] have shown H_2O concentrations to alter by 1–2%, even in melt inclusions that were calculated to have been trapped at the same pressure and erupted at the same monogenetic vent. Variations of this magnitude have been shown here to have a significant effect on the ascent dynamics of magma, and hence the eruptive activity. If this level of variance is evident in a relatively simple geological scenario, the potential degree or variability in the more complex, long-lived silicic volcanic systems considered in this study is likely to be much greater.

There are several other parameters that have also been identified as of principal importance to conduit flow dynamics. Looking at Figure 13 it can be seen that the crystal content, temperature, pressure within the magma chamber, melt composition and conduit geometry all have a significant effect on the modeled ascent velocities. These are all fundamental parameters in most conduit flow models, including the one presented here. However, the knowledge of how homogeneous these properties are within a volcanic system or how they evolve over the active lifetime of a volcanic event does not match the degree to which small changes in these parameters have been shown to alter the results of the presented model. This is particularly the case for the conduit geometry, where although fossilized conduits have been studied in the field and modeling has been carried out to asses the effect of how different shapes or changes in shape effect the volcanic system [e.g., *Costa et al.*, 2007; *Hautmann et al.*, 2009; *Thomas and Neuberg*, 2012], there is no direct observation of this parameters for active volcanic conduits. Consequently, rather than looking at fine details which are interesting, but in terms of effecting the bulk flow properties, relatively insignificant, we believe more effort needs to go into modeling and understanding the areas identified above and seen in Figure 13 that have the biggest effect on ascent dynamics.

In terms of volcano monitoring we need to consider the relationship between essential model parameters (and their required accuracy) and observational data that can be acquired with matching precision. It is now routine to measure seismicity, volatiles and deformation, and to use these data to assess volcanic hazard. While there are multiple types of seismicity associated with volcanos, concentrating on long-period seismicity, and assuming its source mechanism is the brittle failure of the melt then both seismicity and deformation can be used as proxies for magma movement [e.g., *Green et al.*, 2006; *Thomas and Neuberg*, 2012] and both have the potential to be used in forecasting volcanic activity. While deformation has the potential to indicate even small amounts of magma movement, seismicity generated by the mechanism considered here will only occur once the system has already passed a critical point and certain ascent rate has been reached. This in itself may form the basis of a useful predictive tool because as previously discussed there is a potential threshold of ascent velocity that could indicate a switch from effusive to explosive behavior. In addition, although not coincided in the model presented here, it is possible that once ascent rates reach high enough values that viscous dissipation (shear heating) may become significant. This would move magma away from the glass transition, despite increasing shear rates [e.g., *Gonnermann and Manga*, 2007]. In this case a sudden absence of seismicity may indicate accelerating ascent rates. However, if it were possible to detect any changes in the key parameters preceding changes in the rate of long-period seismic swarms then a potential early warning that the current state of volcanic activity may change could be issued.

Of the key parameters identified, changes in the conduit geometry, crystal content and melt composition are difficult to obtain in active system for a variety of reasons. This leaves increases in pressure of the source region (P_e) and the initial dissolved water content ($W_\%$) as the two parameters studied that have the potential to most useful. Changes in P_e will likely produce deformation signals from deep sources in the region of crustal magma chambers. These signals are an indication of changes in the volcanic system, but at this stage there may be no direct link to surface activity. There are many recorded cases of deformation at volcanic centres with no associated eruption [e.g., *Pagli et al.*, 2006], so these deformation signals are potentially most useful in the long-term analysis of prospective volcanic activity.

Measurements of water content are typically obtained through analysis of volcanic glasses or melt inclusions [e.g., *Barclay et al.*, 1998; *Villemant et al.*, 2003]. As this requires sample collection, for active volcanoes this is difficult, dangerous or impossible, and therefore may not lend itself to use in the short-term monitoring of volcanoes. However, H_2O is one of the most volumetrically important constituents in volcanic plumes [*Horrocks et al.*, 2003]. This suggests that changes in $W_\%$ within the magmatic system will likely cause variations in the degassing behavior. The problem is that H_2O within volcanic plumes has traditionally eluded measurement because of large background atmospheric concentrations [*Burton et al.*, 2000], the potential addition of meteoric H_2O [*Lopez et al.*, 2013] and the resulting large measurement uncertainties. Despite these problems it is possible to measure the H_2O flux at active volcanoes [e.g., *Burton et al.*, 2000; *Lopez et al.*, 2013], and therefore it should also be possible to use these data for monitoring purposes. *Lopez et al.* [2013] demonstrated the applicability of including H_2O flux data into monitoring tools at Bezymianny volcano and interpreted a high H_2O flux and high H_2O/CO_2 ratios as an indicator of shallow magma degassing, owing to the fact that H_2O exsolves at relatively low pressures. However, systems like Bezymianny and

Soufrière Hills exhibit open system degassing, where the exsolved gases are able to separate from the melt and ascend through the magma via a permeable network to degas at the surface. *Edmonds et al.* [2010] suggest such pervasive permeability extending to several kilometres depth within the conduit and magma storage system at Soufrière hills in explaining the excess sulphur emitted in the volcanic gasses. It stands to reason that if a water rich magma is introduced to the deep system then the same mechanisms could allow the increased emission of water vapour at the surface, without the need for the degassing magma to be at a shallow level, particularly if such increases are observed without any complimentary evidence to suggest shallow magma intrusion. This could be used as an indicator of whether the water content within the system is increasing or decreasing.

Ultimately, the results of this study indicate that the water and potentially other volatile contents of the magma have the most important influence on driving magma ascent through an established conduit system. There is thus a need, through both monitoring and theoretical studies to better understand dynamic changes in volatile content within a volcanic system.

References

Barclay, J., M. Rutherford, M. Carroll, M. Murphy, and J. Devine (1998), Experimental phase equilibria constraints on pre-eruptive storage conditions of the Soufrière Hills magma, *Geophys. Res. Lett.*, *25*, 3437–3440, doi:10.1029/98GL00856.

Bottinga, Y., and D. F. Weill (1972), Viscosity of magmatic silicate liquids—Model for calculation, *Am. J. Sci.*, *272*(5), 438–475.

Burgisser, A., S. Poussineau, L. Arbaret, T. H. Druitt, T. Giachetti, and J.-L. Bourdier (2010), Pre-explosive conduit conditions of the 1997 Vulcanian explosions at Soufrière Hills Volcano, Montserrat: I. Pressure and vesicularity distributions, *J. Volcanol. Geotherm. Res.*, *194*, 27–41, doi:10.1016/j.jvolgeores.2010.04.008.

Burton, M. R., C. Oppenheimer, L. A. Horrocks, and P. W. Francis (2000), Remote sensing of CO_2 and H_2O emission rates from Masaya volcano, Nicaragua, *Geology*, *28*, 915–918, doi:10.1130/0091-7613(2000)28<915:RSOCAH>2.0.CO;2.

Candela, P. A. (1991), Physics of aqueous phase evolution in plutonic environments, *Am. Mineral.*, *76*(7), 1081–1091.

Castro J. M., and Gardner, J. E. (2008), Did magma ascent rate control the explosive-effusive transition at the Inyo volcanic chain, California?, *Geology*, *36*, 279–282, doi:10.1130/G24453A.1.

Cluzel, N., D. Laporte, A. Provost, and I. Kannewischer (2008), Kinetics of heterogeneous bubble nucleation in rhyolitic melts: Implications for the number density of bubbles in volcanic conduits and for pumice textures, *Contrib. Mineral Petrol.*, *156*, 745–763, doi:10.1007/s00410-008-0313-1.

Collier, L., and J. Neuberg (2006), Incorporating seismic observations into 2D conduit flow modelling, *J. Volcanol. Geotherm. Res.*, *152*, 331–346, doi:10.1016/j.jvolgeores.2005.11.009.

Costa, A., Melnik, O., and R. S. J., Sparks (2007), Controls of conduit geometry and warlock elasticity on lava dome eruptions, *Earth Planet. Sci. Lett.*, *260*, 137–151, doi:10.1016/j.epsl.2007.05.024.

Costa, A., L. Caricchi, and N. Bagdassarov (2009), A model for the rheology of particle-bearing suspensions and partially molten rocks, *Geochem. Geophys. Geosyst.*, *10*, Q03010, doi:10.1029/2008GC002138.

de' Michieli Vitturi, M., A. B. Clarke, A. Neri, and B. Voight (2008), Effects of conduit geometry on magma ascent dynamics in dome-forming eruptions, *Earth Planet. Sci. Lett.*, *272*, 567–578, doi:10.1016/j.epsl.2008.05.025.

de' Michieli Vitturi, M., A. B. Clarke, A. Neri, and B. Voight (2010), Transient effects of magma ascent dynamics along a geometrically variable dome-feeding conduit, *Earth Planet. Sci. Lett.*, *295*, 541–553, doi:10.1016/j.epsl.2010.04.029.

Del Bello, E., E. W. Llewellin, J. Taddeucci, P. Scarlato, and S. J. Lane (2012), An analytical model for gas overpressure in slug-driven explosions: Insights into Strombolian volcanic eruptions, *J. Geophys. Res.*, *117*, B02206, doi:10.1029/2011JB008747.

Devine, J. D., M. D. Murphy, M. J. Rutherford, J. Barclay, R. S. J. Sparks, M. R. Carroll, S. R. Young, and J. E. Gardner (1998), Petrologic evidence for pre-eruptive pressure-temperature conditions, and recent reheating, of andesitic magma erupting at the Soufrière Hills Volcano, Montserrat, W.I., *Geophys. Res. Lett.*, *25*, 3669–3672, doi:10.1029/98GL01330.

Devine, J. D., M. J. Rutherford, G. E. Norton, and S. R. Young (2003), Magma storage region processes inferred from geochemistry of Fe-Ti oxides in andesitic magma, Soufrière Hills Volcano, Montserrat, WI, *J. Petrol.*, *44*, 1375–1400, doi:10.1093/petrology/44.8.1375.

Edmonds, M., A. Aiuppa, M. Humphreys, R. Moretti, G. Giudice, R. S. Martin, R. A. Herd, and T. Christopher (2010), Excess volatiles supplied by mingling of mafic magma at an andesite arc volcano, *Geochem. Geophys. Geosyst.*, *11*, Q04005, doi:10.1029/2009GC002781.

Giachetti, T., T. H. Druitt, A. Burgisser, L. Arbaret, and C. Galven (2010), Bubble nucleation, growth and coalescence during the 1997 Vulcanian explosions of Soufrière Hills Volcano, Montserrat, *J. Volcanol. Geotherm. Res.*, *193*, 215–231, doi:10.1016/j.jvolgeores.2010.04.001.

Giordano, D., J. K. Russell, and B. D. Dingwell (2008), Viscosity of magmatic liquids: A model, *Earth Planet. Sci. Lett.*, *271*, 123–134, doi:10.1016/j.epsl.2008.03.038.

Gonnermann, H. M., and M. Manga (2007), The fluid mechanics inside a volcano, *Annu. Rev. Fluid Mech.*, *39*, 321–356, doi:10.1146/annurev.fluid.39.050905.110207.

Gotto, A. (1999), A new model for volcanic earthquake at Unzen Volcano: Melt rupture model, *Geophys. Res. Lett.*, *26*, 2541–2544, doi:10.1029/1999GL900569.

Green, D. N., J. Neuberg, and V. Cayol (2006), Shear stress along the conduit wall as a plausible source of tilt at Soufrière Hills volcano, Montserrat, *Geophys. Res. Lett.*, *33*, L10306, doi:10.1029/2006GL025890.

Hammer, C., and J. W. Neuberg (2009), On the dynamical behaviour of low-frequency earthquake swarms prior to a dome collapse of Soufrière Hill volcano, Montserrat, *Geophys. Res. Lett.*, *36*, L06305, doi:10.1029/2008GL036837.

Hammer, J. E. (2008), Experimental studies of the kinetics and energetics of magma crystallization, *Rev. Mineral. Geochem.*, *69*, 9–59, doi:10.2139/rmg.2008.69.2.

Hautmann, S., J. Gottsmann, R. S. J. Sparks, A. Costa, O. Melnik, and B. Voight (2009), Modelling ground deformation caused by oscillating overpressure in a dyke conduit at Soufrière Hills Volcano, Montserrat, *Tectonophysics*, *471*, 87–95, doi:10.1016/j.tecto.2008.10.021.

Horrocks, L. A., C. Oppenheimer, M. R. Burton, and H. Duffell (2003), Compositional variation in tropospheric volcanic gas plumes: Evidence from ground-based remote sensing, in *Volcanic Degassing, Geol. Soc. Spec. Publ. 213*, edited by C. Oppenheimer et al., pp. 349–369, The Geological Society, London, U. K.

Hui, H., and Y. Zhang (2007), Towards a general viscosity equation for natural anhydrous and hydrous silicate melts, *Geochim. Cosmochim. Acta*, *71*, 403–416, doi:10.1016/j.gca.2006.09.003.

Humphreys M. C. S., T. Menand, J. D. Blundy, and K. Klimm (2008), Magma ascent rates in explosive eruptions: Constraints from H2O diffusion in melt inclusions, *Earth Planet. Sci. Lett.*, *270*, 25–40, doi:10.1016/j.epsl.2008.02.04.1.

Hurwitz, S., and O. Navon (1994), Bubble nucleation in rhyolitic melts: Experiments at high pressure, temperature, and water content, *Earth Planet. Sci. Lett.*, *122*, 267–280, doi:10.1016/0012-821X(94)90001-9.

Ida, Y. (2007), Driving force of lateral permeable gas flow in magma and the criterion of explosive and effusive eruptions, *J. Volcanol. Geotherm. Res.*, *162*, 172–1845, doi:10.1016/j.jvolgeores.2007.03.005.

Ishibashi, H. (2009), Non-Newtonian behavior of plagioclase-bearing basaltic magma: Subliquidus, viscosity measurement of the 1707 basalt of Fuji volcano, Japan, *J. Volcanol. Geotherm. Res.*, *181*, 78–88, doi:10.1016/j.jvolgeores.2009.01.004.

Ittai, K., L. Vladimr, and O. Navon (2011), Bubble growth in visco-elastic magma: Implications to magma fragmentation and bubble nucleation, *Bull. Volcanol.*, *73*(1), 39–54, doi:10.1007/s00445-010-0402-7.

Johnson, E. R., P. J. Wallace, K. V. Cashman, and H. D. Granados (2010), Degassing of volatiles (H2O, CO2, S, Cl) during ascent, crystallization, and eruption at mafic monogenetic volcanoes in central Mexico, *J. Volcanol. Geotherm. Res.*, *197*, 225–238, doi:10.1016/j.jvolgeores.2010.02.017.

Lensky, N. G., V. Lyakhovsky, and O. Navon (2002), Expansion dynamics of volatile-supersaturated liquids and bulk viscosity of bubbly magmas, *J. Fluid Mech.*, *460*, 39–56, doi:10.1017/S0022112002008194.

Liu, Y., Y. Zhang, and H. Behrens (2005), Solubility of H2O in rhyolitic melts at low pressures and a new empirical model for mixed H20-CO2 solubility in rhyolitic melts, *J. Volcanol. Geotherm. Res.*, *143*, 19–235, doi:10.1016/j.jvolgeores.2004.09.019.

Llewellin, E., and M. Manga (2005), Bubble suspension rheology and implications for conduit flow, *J. Volcanol. Geotherm. Res.*, *143*, 205–217, doi:10.1016/j.jvolgeores.2004.09.018.

Llewellin E. W., H. M. Mader, and S. D. R. Wilson (2002), The constitutive equation and flow dynamics of bubbly magmas, *Geophys. Res. Lett.*, *29*(24), 2170, doi:10.1029/2002GL015697.

Lopez, T., S. Ushakov, P. Izbekov, F. Tassi, C. Cahill, N. Owen, and C. Werner (2013), Constraints on magma processes, subsurface conditions, and total volatile flux at Bezymianny Volcano in 2007–2010 from direct and remote volcanic gas measurements, *J. Volcanol. Geotherm. Res.*, *263*, 92–107, doi:10.1016/j.jvolgeores.2012.10.015.

Lyakhovsky, V., S. Hurwitz, and O. Navon (1996), Bubble growth in rhyolitic melts: Experimental and numerical investigation, *Bull. Volcanol.*, *58*(1), 19–32, doi:10.1007/s004450050122.

Marsh, B. (1981), On the crystallinity, probability of occurrence, and rheology of lava and magma: Contributions to mineralogy and petrology, *Bull. Volcanol.*, *78*, 85–98, doi:10.1007/BF00371146.

Marti, I., O. Höfler, P. Fischer, and E. J. Windhab (2005), Rheology of concentrated suspensions containing mixtures of spheres and fibers, *Rheol. Acta*, *44*, 502–512, doi:10.1007/s00397-005-0432-9.

Melnik, O., A. A. Barmin, and R. S. J. Sparks (2005), Dynamics of magma flow inside volcanic conduits with bubble overpressure buildup and gas loss through permeable magma, *J. Volcanol. Geotherm. Res.*, *143*, 53–68, doi:10.1016/j.jvolgeores.2004.09.010.

Mueller, S., O. Melnik, O. Spieler, B. Scheu, and B. Dingwell (2005), Permeability and degassing of dome lavas undergoing rapid decompression: An experimental determination, *Bull. Volcanol.*, *67*, 526–538, doi:10.1007/s00445-004-0392-4.

Murphy, M. D., R. S. J. Sparks, J. Barclay, M. R., Carroll, and T. S. Brewer (2000), Remobilization of andesite magma by intrusion of mafic magma at the Soufrière Hills Volcano, Montserrat, West Indies, *J. Petrol.*, *41*, 21–42, doi:10.1093/petrology/41.1.21.

Neuberg, J. W., H. Tuffen, L. Collier, D. Green, T. Powell, and D. Dingwell (2006), The trigger mechanism of low-frequency earthquakes on Montserrat, *J. Volcanol. Geotherm. Res.*, *153*, 37–50, doi:10.1016/j.jvolgeores.2005.08.008.

Okumura, S., M. Nakamura, T. Nakano, K. Uesugi, and A. Tsuchiyama (2010), Shear deformation experiments on vesicular rhyolite: Implications for brittle fracturing, degassing, and compaction of magmas in volcanic conduits, *J. Geophys. Res.*, *115*, B06201, doi:10.1029/2009JB006904.

Oppenheimer, C., D. M. Pyle, and J. Barclay (Eds.) (2003), *Volcanic Degassing, Geol. Soc. Spec. Publ. 213*, The Geological Society, London, U. K.

Pagli, C., F. Sigmundsson, T. Arnadottir, P. Einarsson, and E. Sturkell (2006), Deflation of the Askja volcanic system: Constraints on the deformation source from combined inversion of satellite radar interferograms and GPS measurements, *J. Volcanol. Geotherm. Res.*, *152*, 97–108, doi:10.1016/j.jvolgeores.2005.09.014.

Pal, R. (2003), Rheological behaviour of bubble-bearing magmas, *Earth Planet. Sci. Lett.*, *207*, 165–179, doi:10.1016/S0012-821X(02)01104-4.

Rintoul, M. D., and S. Torquato (1997), Precise determination of the critical threshold and exponents in a three-dimensional continuum percolation model, *J. Phys. A Math. Gen.*, *30*(16), L585–L592, doi:10.1088/0305-4470/30/16/005.

Romano, C., J. E. Mungall, T. Sharp, and D. B., Dingwell (1996), Tensile strengths of hydrous vesicular glasses: An experimental study, *Am. Mineral.*, *81*, 1148–1154.

Rust, A. C., and K. V. Cashman (2011), Permeability controls on expansion and size distributions of pyroclasts, *J. Geophys. Res.*, *116*, B11202, doi:10.1029/2011JB008494.

Rutherford, M. J., and J. D. Devine (2003), Magmatic conditions and magma ascent as indicated by hornblende phase equilibria and reactions in the 1995–2002 Soufrière hills magma, *J. Petrol.*, *44*(8), 1433–1454, doi:10.1093/petrology/44.8.1433.

Ryan, G. A., S. C. Loughlin, M. R. James, L. D. Jones, E. S. Calder, T. Christopher, M. H. Strutt, and G. Wadge (2010), Growth of the lava dome and extrusion rates at Soufrière Hills Volcano, Montserrat, West Indies: 2005–2008, *Geophys. Res. Lett.*, *37*, L00E08, doi:10.1029/2009GL041477.

Shaw, H. R. (1972), Viscosities of magmatic silicate liquids—Empirical method of prediction, *Am. J. Sci.*, *272*(9), 870–893.

Snyder, D. (2000), Thermal effects of the intrusion of basaltic magma into a more silicic magma chamber and implications for eruption triggering, *Earth Planet. Sci. Lett.*, *175*, 257–273, doi:10.1016/S0012-821X(99)00301-5.

Sparks, R. S. J., M. D. Murphy, A. M. Lejeune, R. B. Watts, J. Barclay, and S. R. Young (2000), Control on the emplacement of the andesite lava dome of the Soufrière Hills volcano, Montserrat by degassing-induced crystallization, *Terra Nova*, *12*, 14–20.

Taddeucci, J., O. Spieler, M. Ichihara, D. B. Dingwell, and P. Scarlato (2006), Flow and fracturing of viscoelastic media under diffusion-driven bubble growth: An analogue experiment for eruptive volcanic conduits, *Earth Planet. Sci. Lett.*, *243*, 771–785, doi:10.1016/j.espl.2006.01.011.

Thomas, M. E., and J. W. Neuberg (2012), What makes a volcano tick—A first explanation of deep multiple seismic sources in ascending magma, *Geology*, *40*, 351–354, doi:10.1130/G32868.1.

Tuffen, H., and D. Dingwell (2005), Fault textures in volcanic conduits: Evidence for seismic trigger mechanisms during silicic eruptions, *Bull. Volcanol.*, *67*(4), 370–387, doi:10.1007/s00445-004-0383-5.

Tuffen, H., D. B. Dingwell, and H. Pinkerton (2003), Repeated fracture and healing of silicic magma generate flow banding and earthquakes?, *Geology*, *31*(12), 1089–1092, doi:10.1130/G19777.1.

Tuffen, H., R. Smith, and P. R. Sammonds (2008), Evidence for seismogenic fracture of silicic magma, *Nature*, *453*, 511–514, doi:10.1038/nature06989.

Vetere, F., H. Behrens, J. A. Schuessler, F. Holtz, V. Misiti, and L. Borchers (2008), Viscosity of andesite melts and its implication for magma mixing prior to Unzen 1991–1995 eruption, *J. Volcanol. Geotherm. Res.*, *175*, 208–217, doi:10.1016/j.jvolgeores.2008.03.028.

Villemant, B., G. Boudon, S. Nougrigat, S. Poteaux, and A. Michel (2003), Water and halogens in volcanic clasts: Tracers of degassing processes during Plinian and dome-building eruptions, in *Volcanic Degassing, Geol. Soc. Spec. Publ. 213*, edited by C. Oppenheimer et al., pp. 63–79, The Geological Society, London, U. K.

Wadge, G., R. Herd, G. Ryan, E. S. Calder, and J.-C. Komorowski (2010), Lava production at Soufrière Hills Volcano Montserrat: 1995–2009, *Geophys. Res. Lett.*, *37*, L00E03, doi:10.1029/2009GL041466.

Yoshimura, S., and M. Nakamura (2010), Fracture healing in a magma: An experimental approach and implications for volcanic seismicity and degassing, *J. Geophys. Res.*, *115*, B09209, doi:10.1029/2009JB000834.

Zobin, V. M., J. J. Ramirez, H. Santiago, E. Alatorre, and C. Navarro (2011), Relationship between tilt changes and effusive-explosive episodes at an andesitic volcano: The 2004–2005 eruption at Volcan de Colima, Mexico, *Bull. Volcanol.*, *73*, 91–99, doi:10.1007/s00445-010-0405-4.